NF

NASA Contractor Report 165756

An Experimental Study of Massive Blowing From a Nosetip During Jovian Entry

M.S. Holden

Aerodynamic Research Department
CALSPAN CORPORATION
Advanced Technology Center
Buffalo, NY 14225

CONTRACT NAS1-15948
NOVEMBER 1981

NASA
National Aeronautics and Space Administration

Langley Research Center
Hampton, Virginia 23665

FOREWORD

This research was conducted under Contract No. NAS1-15948, sponsored by the NASA Langley Research Center. The author would like to acknowledge the assistance of Kenneth Sutton of NASA Langley and Dr. Donald W. Boyer, Mr. George R. Duryea and Ms. Shirley J. Sweet of Calspan during the course of this work. The results were presented at the AIAA 16th Annual Thermophysics Conference (June 23-25, 1981; Palo Alto, California) and published as AIAA Paper 81-1070.

AN EXPERIMENTAL STUDY OF MASSIVE BLOWING FROM A NOSETIP DURING JOVIAN ENTRY

Michael S. Holden
Calspan Corporation

SUMMARY

A research program has been conducted to examine the structure and stability of the shock layer and the detailed distribution of heating to a highly blowing blunt body in an environment simulating entry into the Jovian atmosphere. The experimental studies were conducted in the 96-inch Shock Tunnel at Calspan in 80% H_2/20% He gas flow at Mach 12. Measurements were made at blowing rates from $0 < \dot{m}/\rho_\infty u_\infty < 0.7$ using CF_4 as the principal injectant; however, selected measurements were also made with N_2, CO_2 and SF_6 as injectants. High speed photography was used to examine the structure and stability of the shock layer. The experimental studies demonstrated that for low blowing rates, the heating rates in the stagnation region can be enhanced as blowing promotes boundary layer transition. While increasing the blowing rate decreased the surface heating for $0.3 < \dot{m}/\rho_\infty u_\infty < 0.5$, further increases in blowing rates did not significantly lower the heating levels below $C_H/C_{H_o} = 0.1$. For injection ratios below 0.3, we did not observe significant shock layer instability; however, for blowing rates of $0.1 < \dot{m}/\rho_\infty u_\infty < 0.5$, high speed photography suggests that the turbulent viscous layer above the body is highly unsteady and a description of this flow in terms of conventional boundary layer theory may be highly inaccurate. For injection ratios of over 0.5, the viscous layer can become grossly unstable. For a given injection rate, shock layer stability can be increased by increasing the molecular weight of the injectant; however, the thermal protection decreases with increased molecular weight. It is recommended that the theoretical modeling of the viscous layer for high mass addition rates be re-examined in the light of these studies.

INTRODUCTION

Ablative heat shields have been used successfully for many years to achieve the thermal protection of spacecraft and missiles during re-entry into the Earth's atmosphere. Under most practical re-entry conditions, the mass of gas ablated into the boundary layer is a small fraction of the mass flow rate in the inviscid flow [i.e., $\dot{m}/\rho_\infty u_\infty O(0.05)$]. Unlike the conventional re-entry into the Earth's atmosphere, the high energy entry into the He/H_2 atmosphere of Jupiter generates extremely large heating rates in the presence of a relatively light convective heating load. Under these conditions the mass addition from the surface blowing will be a significant fraction of the unit mass flow rate in the inviscid flow. In an earlier experimental investigation conducted at Calspan by Holden[1], high speed schlieren photography and heat transfer measurements were made with a transpiration-cooled large hemispherical nosetip to study the stability of the shock layer for large blowing rates ($0.03 < \frac{\dot{m}}{\rho_\infty u_\infty} < 0.3$). These studies demonstrated that for relatively low blowing rates, the structure of the shock layer is significantly modified by the injectant (see Figure 1) and modeling these flows using conventional boundary layer theory is open to serious question. For high blowing rates ($\dot{m}/\rho_\infty u_\infty > 0.3$), as shown in Figure 2, the shock layer became unstable with the flow exhibiting a pulsating oscillation similar to that exhibited by spiked blunt bodies. In these Calspan studies, air was used as the freestream gas and mixtures of helium and nitrogen (were used to simulate the molecular weight and specific heat of steam) were injected through the porous surface of the model. Thus, a relatively light gas with a high volumetric flow rate was used in these studies. This contrasts with the relatively heavy injectants which must be used to simulate the Jovian entry.

The major objective of earlier studies of transpiration cooling techniques was to evaluate how the blockage heat transfer C_H/C_{H_o} varied with the Mach number, Reynolds number and the physical and chemical properties of the freestream and injectant. The lack of definitive techniques to predict the effectiveness of transpiration/film cooling techniques reflects the lack

of fundamental understanding of turbulent mixing in the presence of mass injection and surface roughness. There is a dearth of data at hypersonic speeds where transpiration cooling is of considerable interest. While experimental studies have been conducted in supersonic flow with flat plates[2,3,4] and cones[5,6,7,8] there has been little work on the transpiration cooling of blunt nosetips. In a recent study by Holden[1], heat transfer and flow field studies were performed to examine the transpiration cooling of a blunt nosetip. A survey of the existing experimental data was made and the correlation shown in Figure 3 was obtained. This correlation indicates that for large blowing rates ($\frac{\dot{m}}{\rho_\infty u_\infty C_{H_0}} > 20$), increased blowing does not significantly improve thermal protection. This may well result from a decrease in the stability of the mixing layer and an increase in the scale of turbulence with increasing blowing. However, Holden's measurements on a spherical nosetip, shown in Figures 4 and 5, suggest that heating levels significantly lower than those found on flat plates and cones were obtained for the higher blowing rates. These latter measurements could be correlated in the form $(C_{H_0} - C_H)/C_{H_0} = \frac{1}{3}\left(\frac{\rho_\infty u_\infty}{\rho_e u_e}\right)^{1/3}\left(\frac{\dot{m}}{\rho_\infty u_\infty C_{H_0}}\right)^{1/3}$. However, for blowing rates of greater than 0.3, the flow became highly unstable and violent fluctuations in the surface heating were observed.

The object of the present program was to examine the fluid mechanical structure and stability of the boundary layer and shock layer ahead of a highly blowing heat shield. Injectants with molecular weights from 44 to 120 were used to examine the effect of the volumetric flow rate on boundary layer structure and shock layer stability. High speed schlieren photographs were used to visualize the flow field. Detailed heat transfer and pressure measurements were made on the surface of the porous model. The experiments were conducted with an 80% H_2/20% He mixture for the freestream to simulate the anticipated environment on Jupiter.

The remaining sections of this report discuss the experimental program, the experimental results and the conclusions. The Model Design, Instrumentation and Experimental Setup section discusses the model design, instrumentation and the experimental setups used. This section also describes the operational and physical modifications that were incorporated into the 96-inch

Shock Tunnel[9] so that it could operate with a H_2/He environment. The Experimental Results and Discussion section presents the results of the experimental program. These results are discussed and compared with those made in earlier studies and empirical correlations. The Conclusions section discusses the implications of the measurements to the modeling of the shock layer flow over highly ablating bodies, and the thermal protection of a transpiration-cooled body with a gaseous injectant.

MODEL DESIGN, INSTRUMENTATION AND EXPERIMENTAL SETUP

Model Arr.' Instrumentation

This study employed a gaseous injection technique patterned after that used by the Aerojet transpiration cooled nosetip (TCNT). In this design, which employs some of the better features of both the transpiration and film cooling techniques, the coolant is injected through a large number of slots distributed uniformly over the hemispherical surface of the model. The slots, from which the injectant flows at a low subsonic speed, are fed from tiny sonic orifices machined at the base of each individual slot. These orifices are fed from eight concentric zones in the model which are in turn fed through eight fast-acting "Valcor" valves from eight reservoirs mounted in a cylindrical body at the base of the nosetip. By controlling the initial pressure in each reservoir, the distribution of the injectant around the sphere can be specified. In these studies, where an 80% H_2/20% He helium mixture was used as the test medium, CF_4 was used as the principal injectant; however, CO_2, N_2 and SF_6 were also employed in studies to evaluate the influence of molecular weight on the character of the flow field. The porous nosetip, the fast acting valve assemblies and the reservoirs are shown mounted in the 96-inch Shock Tunnel in Figure 6. The geometry of the slots and their relative position on the nosetip are shown in Figure 7. The 54 rows of slots are staggered in a 35° swirl extending in an arc back to 50° from the stagnation point. The mass flow rate from the slots in each of the eight annular zones on the model were calibrated with each of the gaseous injectants

used in the experimental studies. Miniature heat transfer gages were developed specifically for this study so that detailed measurements could be made in the "bands" between the slots (see Figure 8). Figure 9 shows the positions of the heat transfer gages in the nose and the routing of the instrumentation through the base of the nosetip. The instrumentation has been concentrated in a 25° segment of the nosetip and positioned in such a manner that they can examine whether significant three-dimensional flow structures are developed in the shock layer. Pairs of heat transfer gages were positioned in the model so that measurements were obtained behind the center of the slot and between the slots at the same radial location. The model was also instrumented with pressure gages to determine the surface pressure and the pressure through the internal porting of the models. Instrumentation locations are shown in Figure 9. The second model used in these studies was a smooth-wall replica of the TCNT shown in Figure 10. The model was highly instrumented along orthogonal rays with thin-film heat transfer and pressure gages. The heat transfer distributions obtained with this model at the basic run conditions used in the experiments with nosetip blowing were used to make the measurements obtained in these experiments nondimensional.

Experimental Facility

The experimental program was conducted in the Calspan 96-inch Shock Tunnel. The shock tunnel has a clear advantage in producing and safely handling the 80% H_2/20% He environment required in these studies; however, there are a number of features which present problems of significant technical difficulty. The extremely large mass injection rates ($\dot{m}/\rho_\infty u_\infty$ as large as 0.7) required for this study can cause an elevation in the test section pressure which leads to flow breakdown unless the shock tunnel is fired immediately after the flow through the transpiration nosetip becomes fully established. Even though the dump tank in the 96-inch Shock Tunnel is very large, for the largest injection rates, maintaining a test section low enough to permit a smooth start requires that the steady flow through the tunnel must be established within 30 milliseconds of the establishment of the steady flow of

injectant through the model. Since the flow of injectant had to be initiated with the same switch used to fire the tunnel, this mandated that the tunnel be fired rapidly with exact repetition. To achieve these objectives, it was necessary to redesign the system through which the hydrogen in the double diaphragm rig was vented to the atmosphere, so the 100,000 standard cubic feet (SCF) of hydrogen could be removed from the tunnel in one minute. Venting hydrogen at this rate directly to the atmosphere is clearly hazardous. We resolved this problem by fabricating a secondary high-pressure reservoir into which hot hydrogen from the tunnel could be dumped and then bled slowly to the atmosphere. In this way, we achieved a repeatability of better than 25 milliseconds in the time between closing the switch to fire the tunnel and the establishment of steady flow through the test section.

Considerable effort was devoted to generating test conditions that not only simulated the fluid-dynamic environment of the Jovian atmosphere but also provided an ample test period. The high Mach numbers required in both the test media (80% H_2/20% He) and the driver gas (heated H_2) made the generation of long run times in an impulse facility inherently difficult. Our earlier studies had suggested that the shock layer over our TCNT model was fully established within 2.0 milliseconds from the data rise, so we decided to use at least 4 milliseconds of steady flow in this study. A typical wave diagram for the driver and driven section of the shock tunnel is shown in Figure 11. Because hydrogen has such a high sound speed, the wave trajectory is relatively flat and the associated transit times are inherently short. To maximize run times, we operated with a low incident-shock Mach number and we tailored the prerun conditions to slow the contact surface after it interacts with the bow shock (i.e., we operated in a tailored interface mode). It can be shown that to operate under tailored conditions, the speeds of sound ahead and behind the contact surfaces a_2 and a_3, respectively, must be related by the equation

$$\frac{a_3}{a_2} = \left[\frac{\gamma_4(\gamma_4-1)\left[1 + \left(\frac{\gamma_4+1}{\gamma_4-1}\right)P_{52}\right]}{\gamma_1(\gamma_1-1)\left[1 + \left(\frac{\gamma_1+1}{\gamma-1}\right)P_{52}\right]} \right]^{0.5} . \qquad (1)$$

To obtain tailoring we must control the temperature of the driver gas and the properties of gases in the driver and driven tubes to achieve a shock Mach number (M_s) at which the pressure behind the reflected shock remains constant until the expansion fan from the driver interacts with the reflected shock. Using Eq. (1) as a guide and with further experimentation, we were able to obtain excellent H_2/H_2, He tailoring as can be seen from the reservoir and pitot pressure traces shown in Figure 12. It can be seen that even operating with hydrogen in the driver and driven tubes, test times of over 8 milliseconds can be obtained. With the increased accuracy of the firing sequence, we were able to initiate the injectant flow so that it was fully established between 10 and 18 milliseconds prior to flow establishment through the tunnel. Since the flow of injectant was controlled by sonic orifices, its flow rate was invariable with tunnel conditions, and we found that the shock layer flow was fully established within 2.0 milliseconds from initiation of flow.

EXPERIMENTAL RESULTS AND DISCUSSION

Flow Visualization

The principal objective of this study was to examine how the structure and stability of the hypersonic shock layer over a porous blunt body, in an environment simulating Jovian entry, is influenced by the rate of mass addition and the molecular weight of the injectant. In addition to the model instrumentation, described in the previous section, we employed high speed photography to examine the shock structure ahead of the body and the boundary layer/mixing layer beneath it. In most experimental studies of blunt body flows at hypersonic speed it is difficult to visually observe the boundary layer or mixing layer on the body because the strong entropy gradients developed across the shock layer mask the density gradients that delineate the edge of the boundary layer. Using high speed photography to visualize the boundary layer over a blunt body depends on correctly illuminating the flow and processing light beam. In this study, we employed circular cut-off with a single pass schlieren system whose focal length was 20 feet. A Hycam high speed camera running at 7000 frames per second was used to obtain

photographs of the flow. Photographs typical of those obtained over the nonblowing body are shown in Figure 13. We were not able to observe a distinct boundary layer embedded within the shock layer. However, when a relatively cold, high-density injectant is introduced at the base of the boundary layer, the turbulent mixing region close to the body can be seen clearly (see Figure 14). The exposure rate on the film was sufficient to "stop" the motion of large scale turbulent structure.

Measurements On The Smooth And Nonblowing Models

As part of the initial phase of this study, we examined flow over the porous nonblowing nosetip (see Figure 6) and the smooth replica of this configuration shown in Figure 10. We wished to determine whether the surface roughness would trip the boundary layer and cause roughness heating augmentation. In an earlier program, measurements were made on both smooth and porous models in air at Mach 11 for a Reynolds number of 10×10^6. We observed boundary layer transition on the smooth configuration close to the sonic point, as shown in Figure 15. On the porous model, transition had been tripped by the roughness close to the stagnation region, and the roughness had apparently enhanced the heating beneath the turbulent boundary layer, as can be seen from Figure 16. The measurements made with smooth and porous models at Mach 11 in the 80% H_2/20% He gas flow at Reynolds numbers of 2×10^6 are shown in Figures 17 and 18. Here it can be seen that the boundary layer remains laminar on the smooth configuration, and the rough surface of the porous model does not trip transition or induce higher than laminar heating rates. Thus, when we observe heating levels on the blowing model that are higher than those with zero mass injection, we must conclude that blowing has tripped the boundary layer inducing turbulent heating.

Photographic Studies Of Shock And Mixing Layer Structure And Stability

The experimental studies were conducted in a 80% H_2/20% He gas flow at a Mach number of 12, with the freestream conditions as listed in Table 1.

Table 2 lists the matrix of model configurations and injection conditions that were used for the runs specified in Table 1. CF_4 was used as the principal injectant in these studies to closely match the molecular weight ratio encountered during Jovian entry. Further studies were performed with N_2, CO_2 and SF_6 as injectants to explore the effect of the molecular weight ratio on the structure and stability of the flow field. While the major segment of the program was conducted with a uniform distribution of blowing around the model, the "theoretical" blowing distribution, as shown in Figure 19, was used to pattern the "peaked" distribution also used in the experimental program.

The photographs of the flow over the smooth and nonblowing porous model shown in Figure 13 do not, as mentioned earlier, provide the viewer with evidence of the size or condition of the boundary layer over the body. However, we know the boundary layer to be laminar from the surface heat transfer measurements discussed previously. The measured shock stand-off distance is in good agreement with theoretical predictions for an 80% H_2/20% He environment (see Figure 20). The first photographic evidence of the size of structure of the boundary layer and its influence on the shock layer occurs for $\dot{m}/\rho_\infty u_\infty = 0.1$. The photographs shown in Figure 21 indicate that the shock stand-off distance has been increased, and the boundary layer, which is just visible, is transitional and turbulent. Increasing the nondimensional blowing rate to 0.3 causes significant increase in the shock stand-off distance, and at this condition the boundary layer/mixing layer is highly visible. Figure 22 was taken at a slightly different cut off and shows that the bow shock has been displaced forward by 0.1 body diameters and the viscous layer now occupies one third of the shock layer. It is clear from the photographs shown in Figures 22 and 23 that the boundary layer is turbulent in the stagnation region, and the scale of the turbulence layer is approximately equal to the thickness of the mixing layer. While the stability and shape of the bow shock does not appear to be strongly influenced by the turbulence over the body, it is clear that a major part of the subsonic inviscid flow in the shock layer is. When $\dot{m}/\rho_\infty u_\infty$ is increased to 0.5, the high speed photographs, shown in Figure 24, clearly demonstrate that both the stability and shape of the bow shock and the structure of the shock layer are strongly influenced by the turbulent mixing layer. The shock layer

flow is not grossly unstable; however, for CF_4 flows with $\dot{m}/\rho_\infty u_\infty > 0.3$, it is clear that a conventional boundary layer approach could not be used in a theoretical model of these flows.

Using the peaked injection profile prescribed in Figure 19, with a maximum blowing rate of 0.5, we obtained the somewhat more stable flow shown in Figure 25. Here, while large scale turbulent fluctuations are evident in the boundary layer, the bow shock appears to be relatively stable. The relative stability of this latter flow encouraged us to perform the remaining experiments for $\dot{m}/\rho_\infty u_\infty = 0.7$ with a peaked injection profile rather than a uniform distribution. The latter, we believe, would cause gross flow instabilities. The high speed photographs (see Figure 26) for the peaked injection with $\dot{m}/\rho_\infty u_\infty = 0.7$ clearly show gross instabilities exist, with what appears to be a circular instability mode. The aerodynamics of a nosetip exhibiting this instability could seriously jeopardize the mission on which it is flown. If a conical afterbody was placed behind the nosetip, on the basis of earlier studies by Holden[10], we would expect that such a phenomenon would cause large and destabilizing effects on the cone stability.

Figure 20a shows the variation of shock standoff distance and the mean thickness of the boundary layer with the mass injection rate of CF_4 for both uniform and "peaked" injection patterns. With zero mass addition, the boundary layer is very thin and, as mentioned earlier, the shock standoff distance is close to the theoretical "inviscid" value for a 80% H_2/20% He freestream. Both the mixing layer thickness and the shock standoff distance increase with increased blowing rate. When a blowing rate of 0.5 is obtained, the mixing layer occupies approximately one-half the thickness of the shear layer. These measurements demonstrate that despite the gross unsteadiness of the mixing layer, the bow shock is effectively displaced ahead of the body by the thickness of the mixing layer. Decreasing the molecular weight of the injectant at a fixed value of $\dot{m}/\rho_\infty u_\infty$ increases the volume of gas introduced into the shock layer and the forward displacement of the bow shock. Figure 20b shows the variation of shock and mixing layer thickness with molecular weight

of the injectant. This figure shows that the lowest molecular weight fills over half the shock layer thickness and is highly unsteady. When SF_6 was used as an injectant, the flow was steadier and the mixing layer occupied over one-third the thickness of the shock layer.

Rather than explore the effects of the molecular weight for $\dot{m}/\rho_\infty u_\infty = 0.7$ where the flow was grossly unstable, we chose to perform these studies for $\dot{m}/\rho_\infty u_\infty = 0.5$, where we believed the flow was incipiently unstable. We employed N_2, CO_2 and SF_6 injectants, with a uniform injection distribution. In addition, the flow for a "peaked" CO_2 distribution was examined. Comparing the high speed photographs of the flow for N_2, CO_2 and SF_6 injectants, shown in Figures 27, 28, and 29, respectively, with those for CF_4 in Figure 24, it can be seen that both the structure of the bow shock and the shear layer become increasingly stable as the molecular weight of the injectant increases. We believe that this results directly from the inverse relationship between the volume of gas injected through the nosetip and its molecular weight for a given $\dot{m}/\rho_\infty u_\infty$. Clearly a much greater volume of N_2 than SF_6 is being injected for the same value of $\dot{m}/\rho_\infty u_\infty$. Again, as shown in Figure 30 for CO_2, we found the flow fields over the models with the "peaked" distribution were significantly more stable than those with uniform blowing. It is clear from these studies that for flows with $\dot{m}/\rho_\infty u_\infty > 0.3$, any theoretical modeling must acknowledge the first order relationships between the shock structure and the structure of the turbulent mixing layer. The interaction between the bow shock and mixing layer, combined with the highly turbulent nature of the mixing layer, is a major reason for the relatively poor thermal protection of the body by the massive amounts of injectant, and will be described in the following section.

Distribution Of Heating In The Presence Of Massive Blowing

The earlier studies of the transpiration cooling of flat plates and cones and, most recently, the studies of spherical nosetips used gaseous injectants whose molecular weights were significantly smaller than that of the freestream, because such gases make the most efficient coolants. However, it was also recognized in these studies that flow instabilities can occur at relatively low blowing rates. In the present study, we used gases which were very heavy compared with the freestream, to obtain the correct Jovian simulation, and while these transpiration-cooled flows should be intrinsically more stable, they also might be expected to be less efficient.

The heat transfer measurements on the smooth and nonblowing models demonstrated, as described earlier, that the flows over both models were fully laminar. Introducing mass into the boundary layer perpendicular to the surface is destabilizing, particularly in the stagnation region, and for the injection rates used in the present studies, we tripped the boundary layer for every configuration tested. The distributions of heat transfer over the porous model with a CF_4 injectant for blowing rates of 0, 0.1, 0.3, 0.5 and 0.7 are shown in Figures 31 and 32 for uniform and "peaked" injection profiles respectively. We see that for blowing rates of 0.1, the boundary layer is tripped by injection, causing the heating rates in the stagnation region to nearly double, while those further downstream remained at their laminar levels. For $\dot{m}/\rho_\infty u_\infty = 0.3$, turbulent flow exists over the nose-caps; however, the heating levels remain at approximately their laminar levels over the entire nosetip. When injection rates equal to 0.5 are used, the heat transfer to the stagnation region of the flow is greatly reduced for both uniform and "peaked" injection profiles (see Figures 32 and 33); however, further downstream, transpiration cooling proved less effective. These measurements are plotted in nondimensional form in Figures 34 and 35, based on laminar nonblowing heating. It is readily apparent that to achieve reductions in heating of a magnitude similar to the "light gas studies," significantly larger nondimensional blowing rates are required, and at these large blowing rates, the flows are

again highly unstable. The measurements with the peaked distributions at the high injection rates, shown in Figure 35, also demonstrate that it is difficult to achieve heat transfer ratios on these configurations below one tenth of the nonblowing level irrespective of the blowing rate.

A comparison between the heat transfer distributions for the gaseous injectants N_2, CO_2, CF_4 and SF_6 with a common blowing rate of 0.5 is shown in Figure 36. We find that the gases with the lower molecular weight are more effective as coolants despite the greater instability of the shock layer for these lighter gases. The heat transfer measurements for the uniform and peaked CO_2 distributions are shown in dimensional and nondimensional form in Figures 37 and 38. Both sets of data show a 90% reduction in heating over the nosetip, which is in agreement with the earlier measurements. As one might have anticipated from the earlier tests, the uniform distribution is more effective in reducing heat transfer than the peak distribution; however, since significantly less gas is involved in cooling the nosetip when a peaked distribution is employed, this latter method of introducing the gas must be considered the most efficient. Considering the unstable nature of the flows depicted in the high speed photographs (see Figures 19 through 29) with $\dot{m}/\rho_\infty u_\infty > 0.5$, it is perhaps surprising that 90% reductions in heating can occur. However, at the large injection rates, we are depositing a large amount of cool gas in front of the body.

CONCLUSIONS

An experimental study has been successfully conducted to examine the structure and stability of the shock layer and the distribution of heating to a highly blowing blunt body in an environment simulating the fluid dynamics of entry into the Jovian atmosphere. In this study, high speed schlieren photography was used to examine the structure and stability of the shock layer and heat transfer, and pressure measurements were obtained on a porous blunt nosetip for blowing rates $0 < \frac{\dot{m}}{\rho_\infty u_\infty} < 0.7$ in a 80% H_2/20% He gas flow. In these studies, which were conducted in the Calspan 96-inch Shock Tunnel at Mach 12,

CF_4 was used as the principal injectant, with N_2, CO_2 and SF_6 used in additional selected studies. The initial studies demonstrated that it was possible to generate an environment in the shock tunnel that simulated the fluid dynamic aspects of the Jovian environment. Flow durations of close to 8 milliseconds were generated in the shock tunnel. This is four times the time required to establish flow over the highly blowing models. While heat transfer measurements both on a smooth replica of the porous nosetip and on the nonblowing porous model indicated that the flow over both these configurations was fully laminar, we observed that for low blowing rates, the heat transfer was enhanced when fluid injection tripped the boundary layer. For blowing rates between 0.1 and 0.5, the heat transfer to the surface decreased; however, further increases in the blowing rate did not result in further reduction of the heating levels below $C_H/C_{H_o} = 0.1$. Detailed photography indicated that for $\dot{m}/\rho_\infty u_\infty$ less than 0.3, the shock layer remains stable, although a description of the flows for $\dot{m}/\rho_\infty u_\infty > 0.1$ indicates that conventional boundary layer theory could be seriously in error. For $\dot{m}/\rho_\infty u_\infty > 0.5$, the shock layer flow can become grossly unstable, with the low molecular weight injectants exhibiting the greatest instability. It is recommended that these measurements be used in an examination of the existing codes used to predict the flow structure and heating on highly blowing nosetips.

REFERENCES

1. Holden, M.S. Studies Of Transpiration Cooling, Surface Roughness And Entropy Swallowing In Transitional And Turbulent Boundary Layers Over Nose Tips XXX Congress International Astronautical Federation Preprint IAF-79-F-42 September 17-22, 1979.

2. Brunner, M. J. Transpiration Cooling Tests At A Sharp Sphere-Cone In A Rocket Exhaust Using N_2, H_e and H_2O Coolants Paper No. 64-WA/Ht-50, ASME Winter Annual Meeting, New York 1964.

3. Pappas, C.C., and Okuno, A.F. Measurements of Heat Transfer And Recovery Factor Of A Compressible Turbulent Boundary-Layer On A Sharp Cone With Foreign Gas Injection NASA TN D-2230 1964.

4. Fogaroli, R.P. Measurements of Turbulent Heat Transfer And Skin Friction Reduction On A Porous Cone With Air Injection At High Mach Numbers General Electric Report No. 64SD5291 1964.

5. Bartle, E.R., and Leadon, B.M. The Effectiveness As A Universal Measure of Mass-Transfer Cooling For A Turbulent Boundary-Layer Proceedings 1962 Heat Transfer And Fluid Mechanics Institute Stanford University Press, Stanford 1962.

6. Danberg, J.E. Characteristics Of The Turbulent Boundary-Layer With Heat And Mass Transfer At Mach Number 6.7 Proceedings 5th U.S. Navy Symposium on Aeroballistics White Oak, Maryland 1961.

7. Spalding, D.B., and Chi, S.W. The Drag Of A Compressible Turbulent Boundary Layer On A Smooth Flat Plate With And Without Heat Transfer J. Fluid Mech., 117-143 1964.

8. Van Driest, E.R. Problem Of Aerodynamic Heating Aeronautical Engineering Review, Vol. 15, No. 10 1956.

9. "Calspan Hypersonic Shock Tunnel, Description And Capabilities Brochure" 1975.

10. Holden, M.S. Accurate Vehicle Experimental Dynamics Program - Studies Of Aero-Thermodynamic Phenomena Influencing The Performance Of Hypersonic Re-Entry Vehicles Calspan Report No. AB-6072-A-2, SAMSO-TR-79-47 August 1979.

SYMBOLS

a	speed of sound
CF_4	carbon tetrafluoride
C_H	coefficient of heat transfer
CO_2	carbon dioxide
H	total enthalpy
He	helium
H_2	hydrogen
K	roughness height
M	Mach number
$\dot{m}$	mass addition rate per unit area of injectant
p	pressure
$\dot{q}$	heat transfer rate
Re	Reynolds number
S	surface
SF_6	sulfur hexafluoride
S/R	surface distance/radius
u,v	velocity
$X_{S/D}$	shock standoff/distance
γ	specific heat ratio
δ/D	mixing layer thickness
ρ	density

Subscripts:

e	edge conditions above the boundary layer
w	conditions at the wall
∞	conditions in the freestream
R	recovery condition
0	smooth wall conditions

Table 1
TEST CONDITIONS

FLOW PROPERTIES \ R	1	2	3	4	5	6	7	8	9	10	11	12	13	14	15	16
M_0	1.850	1.850	1.850	1.840	1.860	1.820	1.880	1.880	1.880	1.900	1.900	1.900	1.900	1.880	1.900	1.931
P_0 (N/m^2)	4.266(7)	5.418(7)	3.223(7)	3.030(7)	3.058(7)	2.966(7)	3.177(7)	3.305(7)	3.287(7)	3.267(7)	3.308(7)	3.284(7)	3.232(7)	3.278(7)	3.308(7)	8.733(7)
H_0 (m^2/sec^2)	7.901(6)	7.901(6)	7.901(6)	7.714(6)	7.889(6)	7.563(6)	8.002(6)	8.040(6)	8.109(6)	8.096(6)	8.140(6)	8.077(6)	8.159(6)	8.071(6)	8.159(6)	8.356(6)
T_0 (°K)	691.1	691.1	691.1	683.3	696.9	670.0	708.9	711.7	718.3	717.2	721.1	715.6	722.8	715.0	722.8	749.9
M_∞	12.69	13.22	11.62	11.61	11.71	11.52	11.35	12.55	12.24	12.36	12.57	11.72	11.73	11.55	11.96	11.48
U_∞ (m/sec)	3.888(7)	3.897(7)	3.883(7)	3.861(7)	3.906(7)	3.822(7)	3.929(7)	3.951(7)	3.965(7)	3.963(7)	3.976(7)	3.952(7)	3.972(7)	3.949(7)	3.975(7)	4.016(7)
T_∞ (°K)	20.84	17.52	22.51	22.31	22.42	22.19	24.16	19.98	21.15	20.72	20.17	22.92	23.11	23.56	22.26	24.67
P_∞ (N/m^2)	459.4	324.9	437.5	414.6	386.3	419.8	500.6	275.2	321.0	299.9	273.2	422.3	413.4	463.6	374.1	547.2
Q_∞ (N/m^2)	4.736 (4)	4.073(4)	4.249(4)	4.017(4)	3.900(4)	3.922(4)	4.638(4)	3.118(4)	3.468(4)	3.286(4)	3.103(4)	4.172(4)	4.091(4)	4.445(4)	3.849(4)	5.187(4)
ρ_∞ (kg/m^2)	0.06267	0.05360	0.05638	0.05391	0.05113	0.05370	0.06009	0.03895	0.04400	0.04196	0.03926	0.05344	0.05195	0.05760	0.04873	0.06422
μ_∞ (N/m-sec)	1.324(-6)	1.119(-6)	1.426(-6)	1.410(-6)	1.414(-6)	1.407(-6)	1.529(-6)	1.298(-6)	1.344(-6)	1.312(-6)	1.282(-6)	1.460(-6)	1.456(-6)	1.481(-6)	1.408(-6)	1.564(-6)
Re/m	1.841(7)	1.968(7)	1.535(7)	1.476(7)	1.412(7)	1.468(7)	1.546(7)	1.247(7)	1.288(7)	1.268(7)	1.218(7)	1.456(7)	1.416(7)	1.519(7)	1.375(7)	1.662(7)

Table 2

TEST MATRIX

RUN	TEST GAS % H_e/% H_2	MODEL CONFIGURATION	$\frac{\dot{m}}{\rho_\infty U_\infty}$	INJECTANT	MODE
1	20/80	POROUS	0.1	CF_4	UNIFORM
2	20/80	POROUS	0.3	CF_4	UNIFORM
3	20/80	POROUS	0.5	CF_4	UNIFORM
4	20/80	POROUS	0.5	CO_2	UNIFORM
5	20/80	POROUS	0.5	CO_2	PEAKED
6	20/80	POROUS	0	–	–
7	20/80	POROUS	0.5	CF_4	PEAKED
8	20/80	POROUS	0.7	CF_4	PEAKED
9	20/80	POROUS	0.5	CF_4	UNIFORM
10	20/80	POROUS	0.3	CF_4	UNIFORM
11	20/80	POROUS	0.5	SF_6	UNIFORM
12	20/80	POROUS	0	–	–
13	20/80	POROUS	0.5	N_2	UNIFORM
14	20/80	POROUS	0.3	CF_4	UNIFORM
15	20/80	POROUS	0	–	–
16	20/80	NONPOROUS	0	–	–

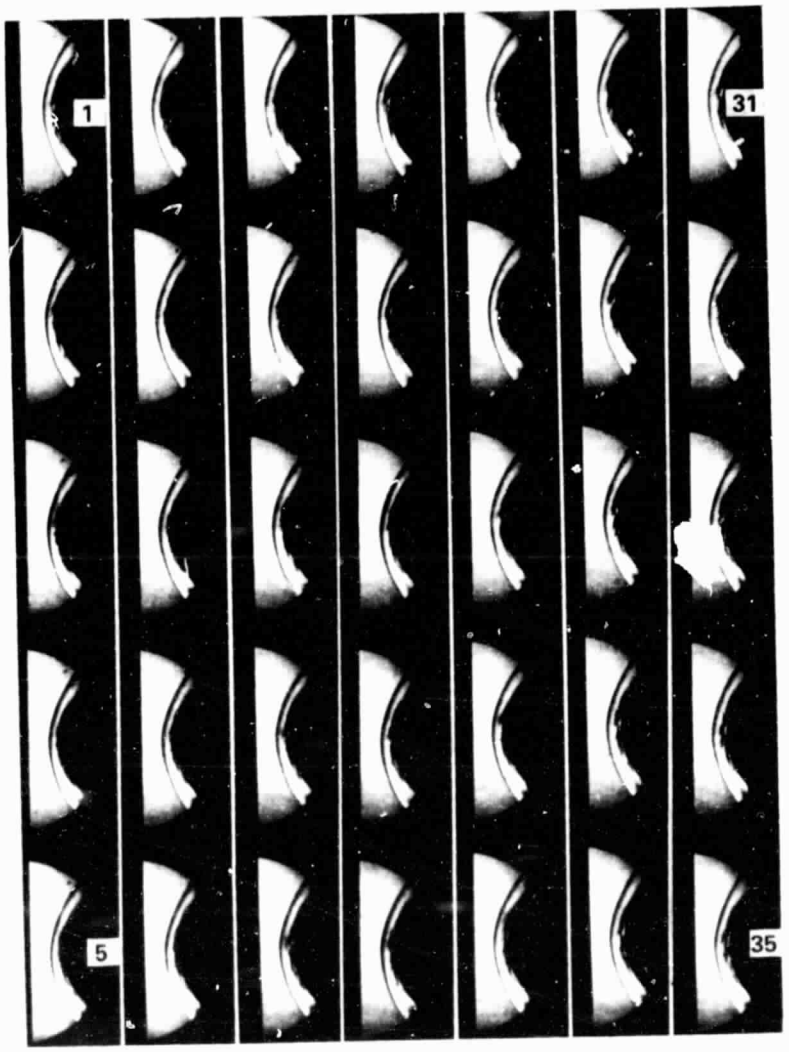

Figure 1 HIGH SPEED PHOTOGRAPHIC SEQUENCE (5000 FRAMES/SEC) SHOWING THE TURBULENT MIXING INJECTANT WITH THE GAS IN THE STEADY SHOCK LAYER

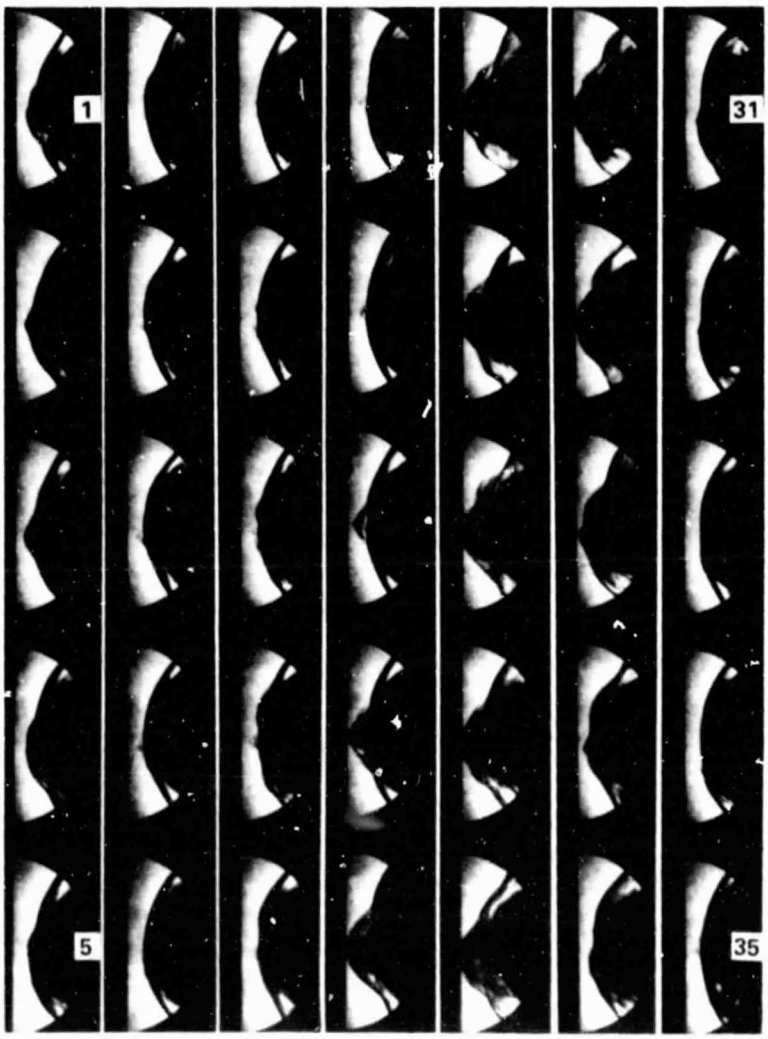

Figure 2 HIGH SPEED PHOTOGRAPHIC SEQUENCE (5000 FRAMES/SEC) SHOWING THE GROSS INSTABILITIES WHICH CAN OCCUR FOR HIGH INJECTANT FLOW RATES

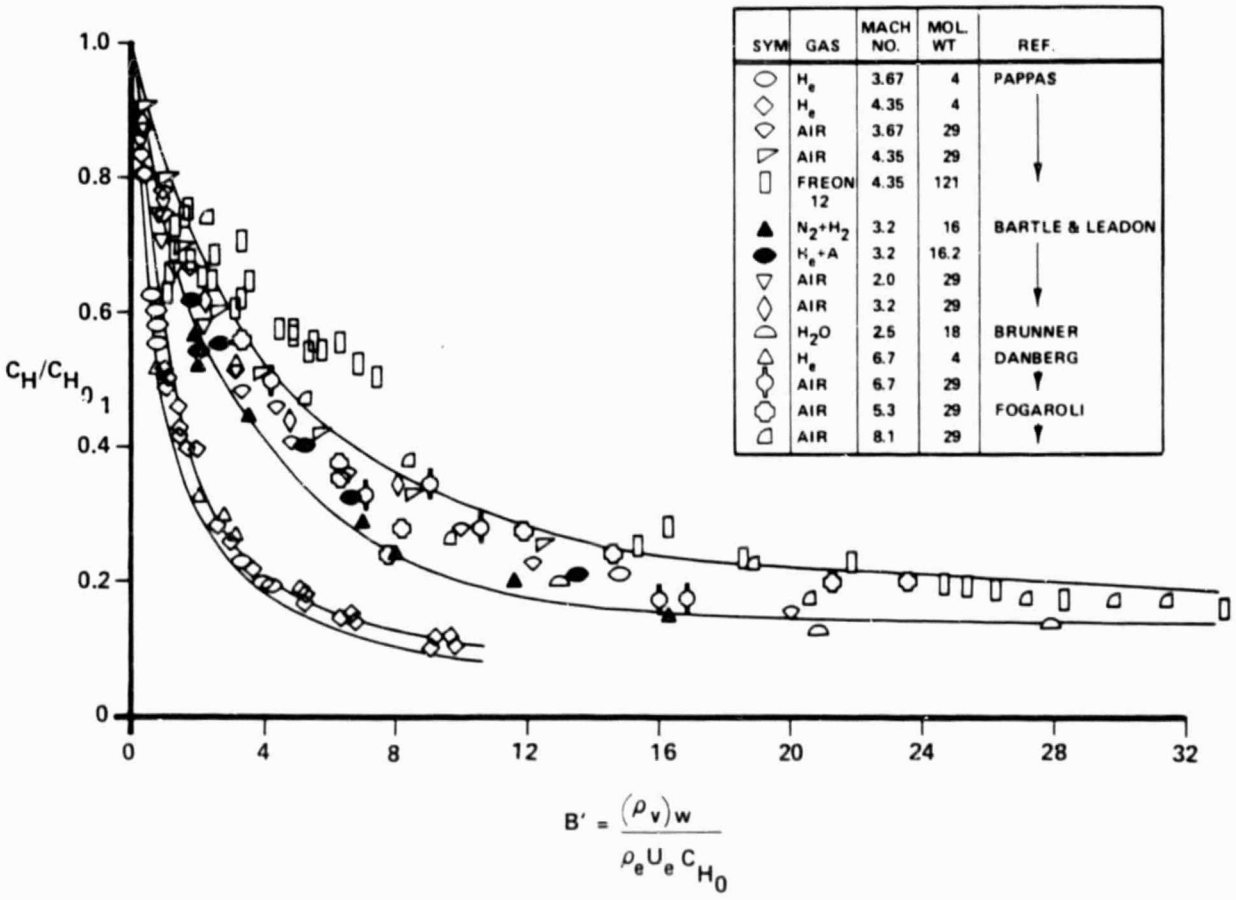

Figure 3 SUMMARY OF BLOCKAGE HEATING FROM EARLIER STUDIES ON FLAT PLATES AND CONES IN TURBULENT FLOW

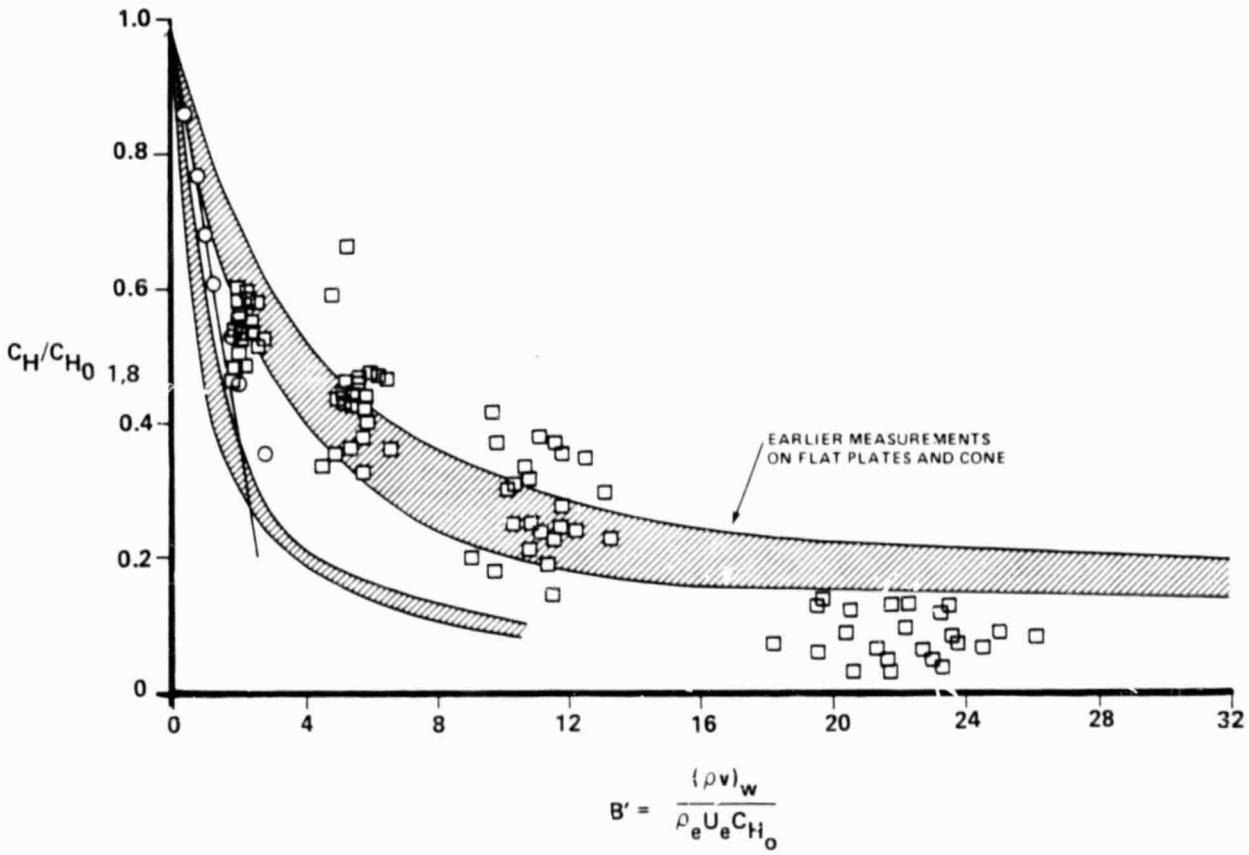

Figure 4 COMPARISON BETWEEN THE MEASUREMENT MADE IN THE CURRENT STUDIES WITH NITROGEN INJECTANT AND THE EARLIER BLOCKAGE DATA

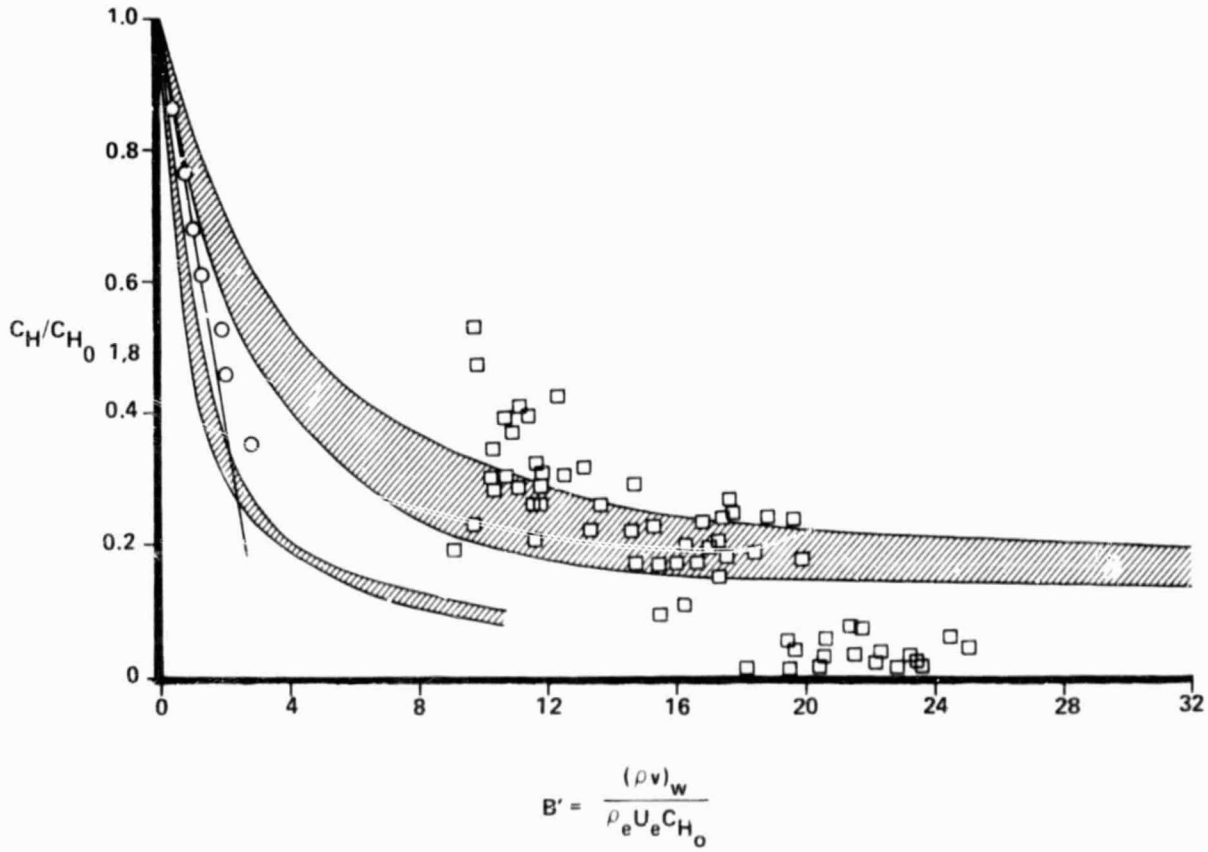

Figure 5 COMPARISON BETWEEN THE MEASUREMENT MADE IN THE CURRENT STUDIES WITH HELIUM/NITROGEN MIXTURE AND THE EARLIER BLOCKAGE DATA

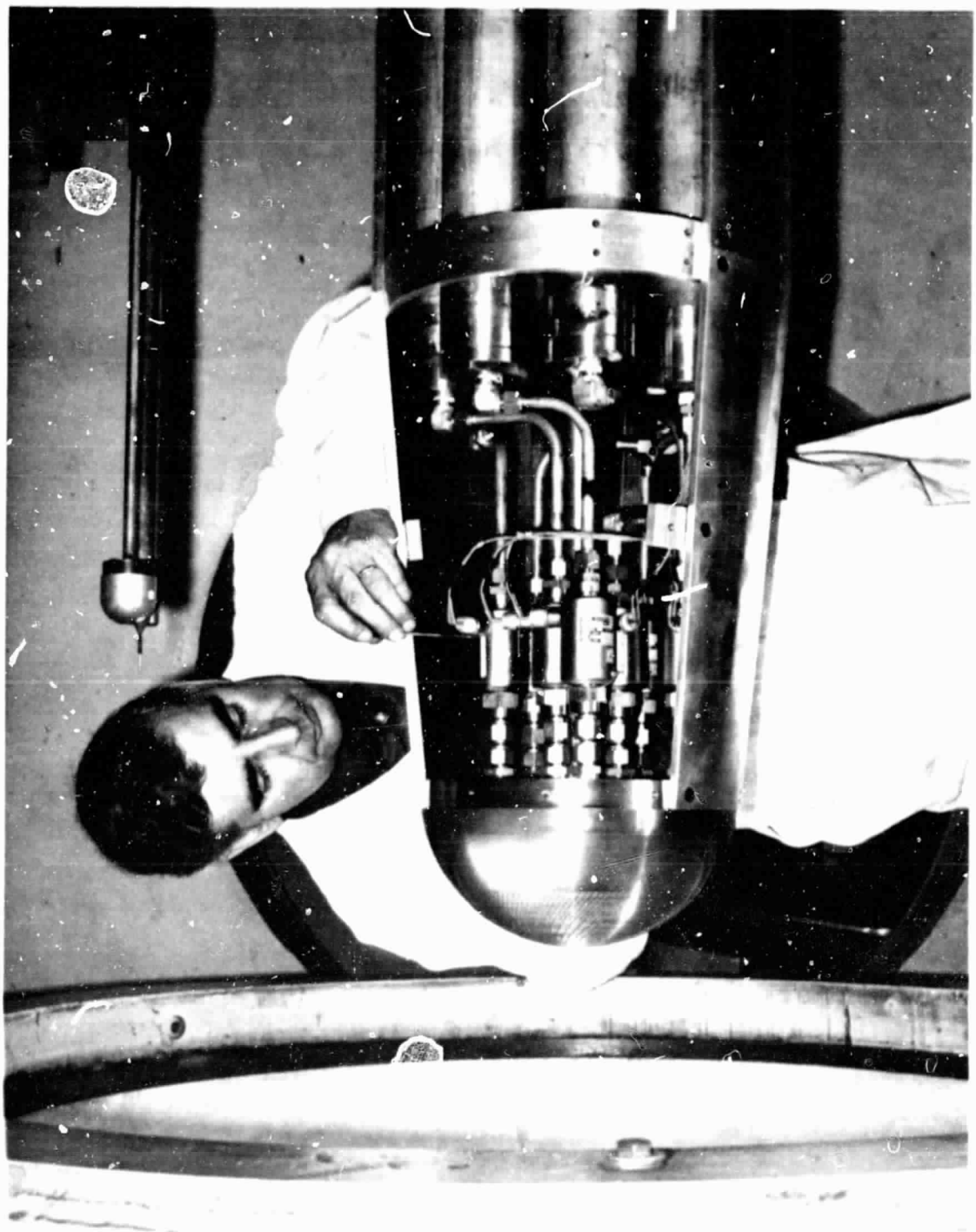

Figure 6 VALCOR VALVE AND RESERVOIR ASSEMBLY

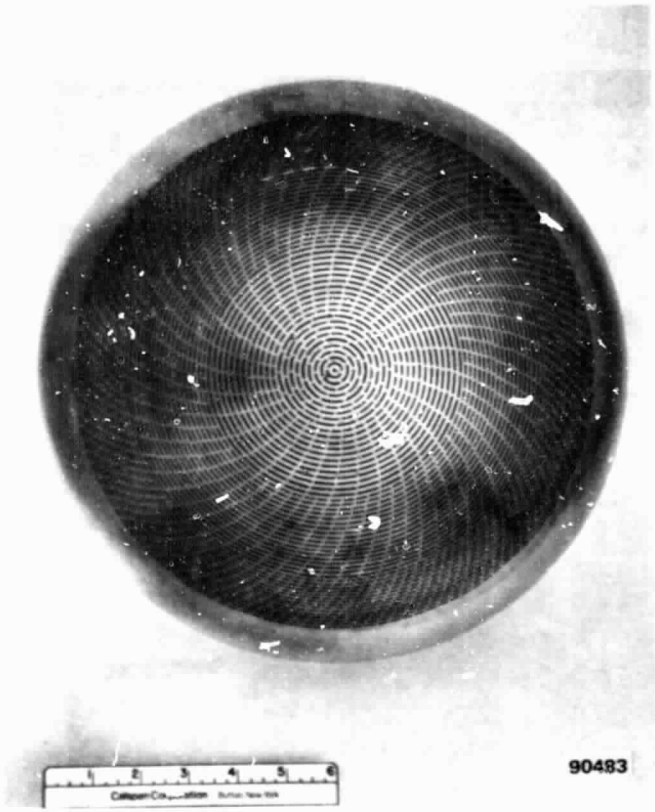

a. FRONT VIEW

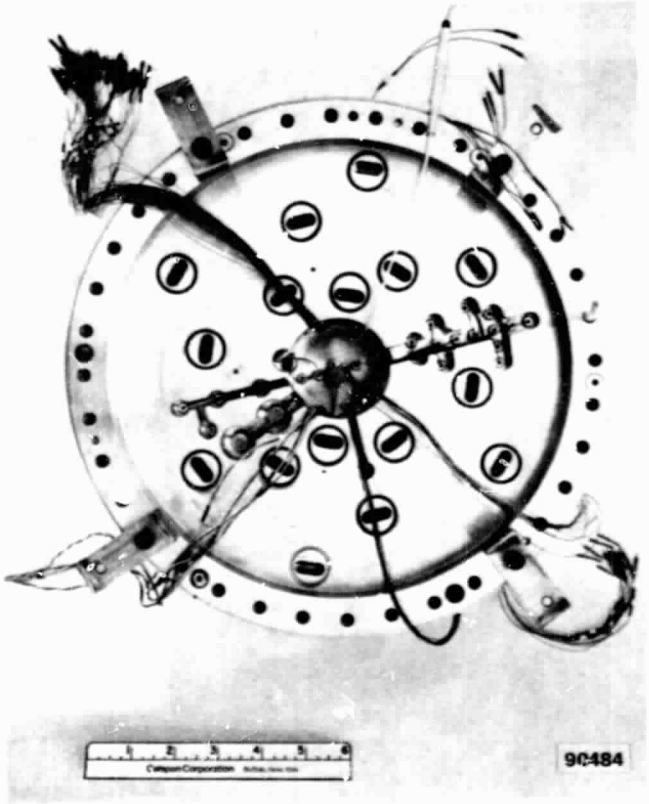

b. BACK VIEW

Figure 7 INSTRUMENTED SCANT NOSE TIP

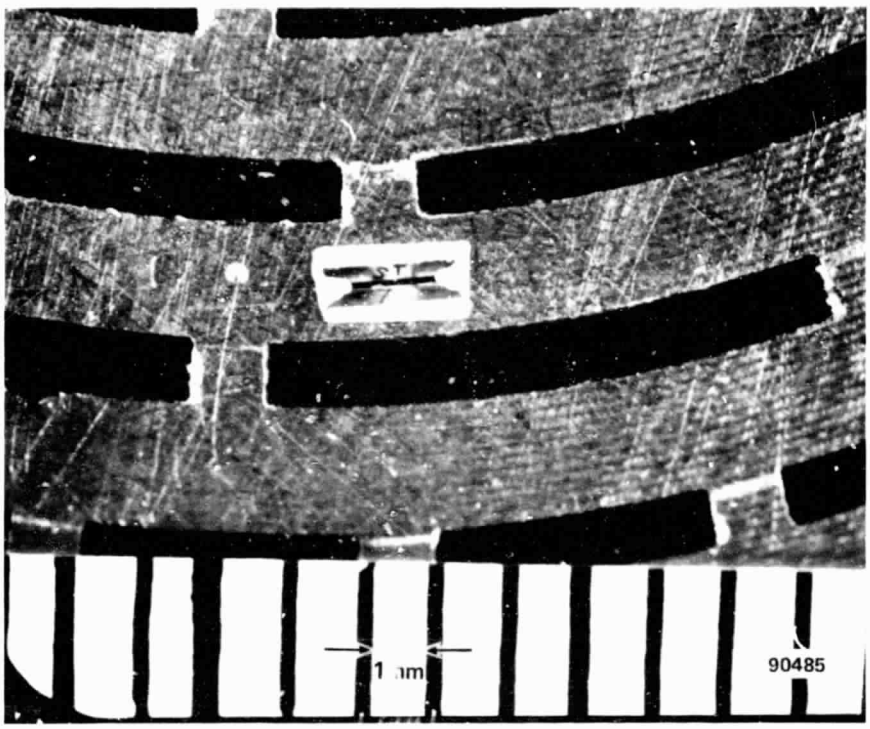

SINGLE ELEMENT

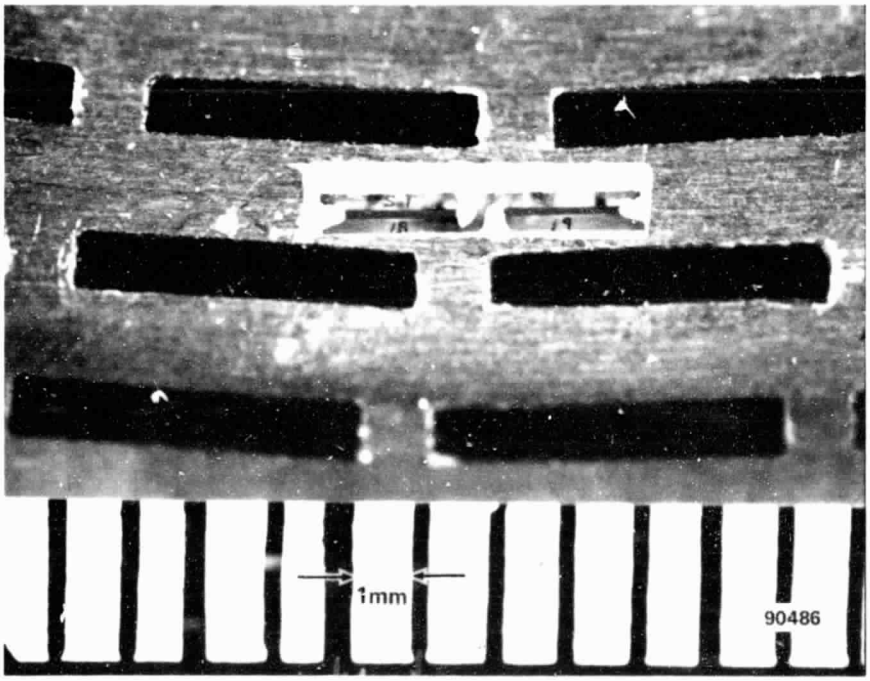

DOUBLE ELEMENT

Figure 8 TYPICAL HEAT TRANSFER GAGE INSTALLATION

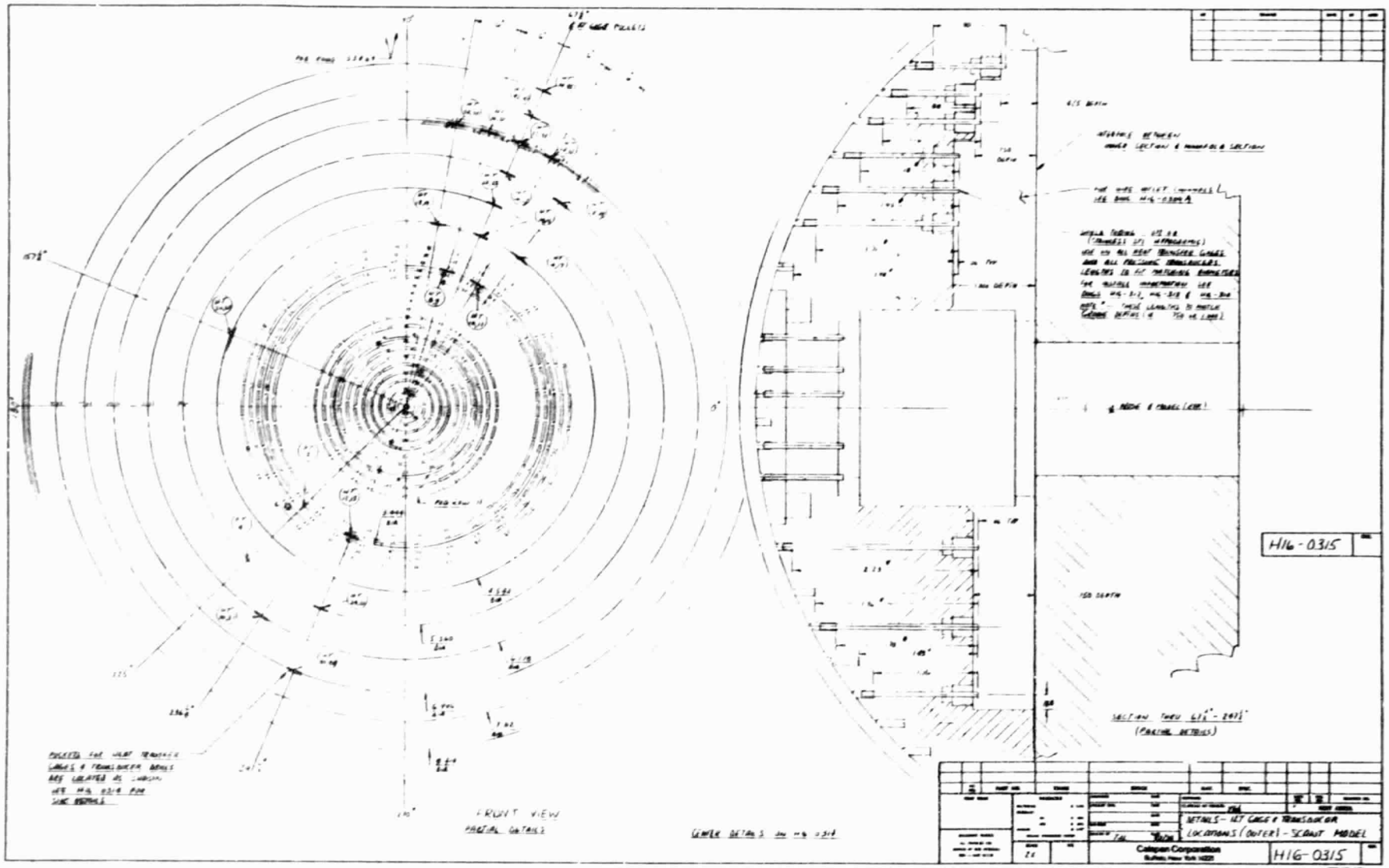

Figure 9 HEAT TRANSFER & PRESSURE GAGE LOCATION ON THE SCANT NOSE TIP

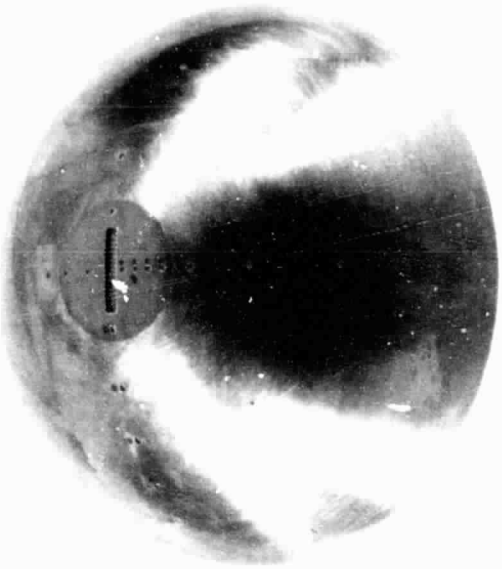

91789

(a)

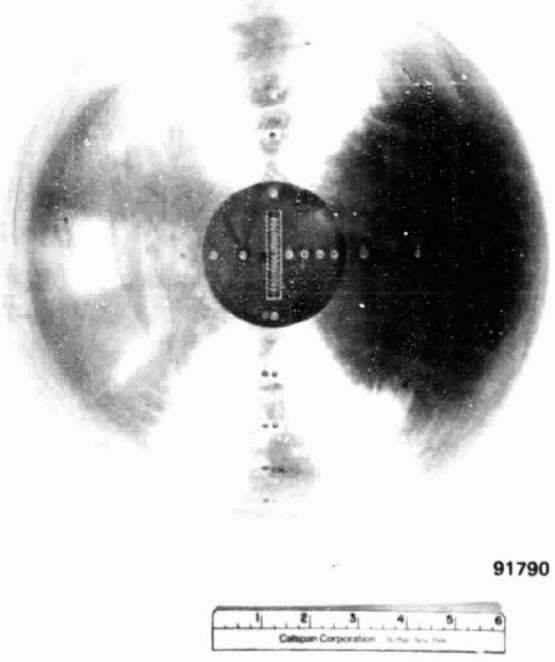

91790

(b)

Figure 10 HEMISPHERICAL MODEL FOR BLUNT BODY TRANSITION STUDIES

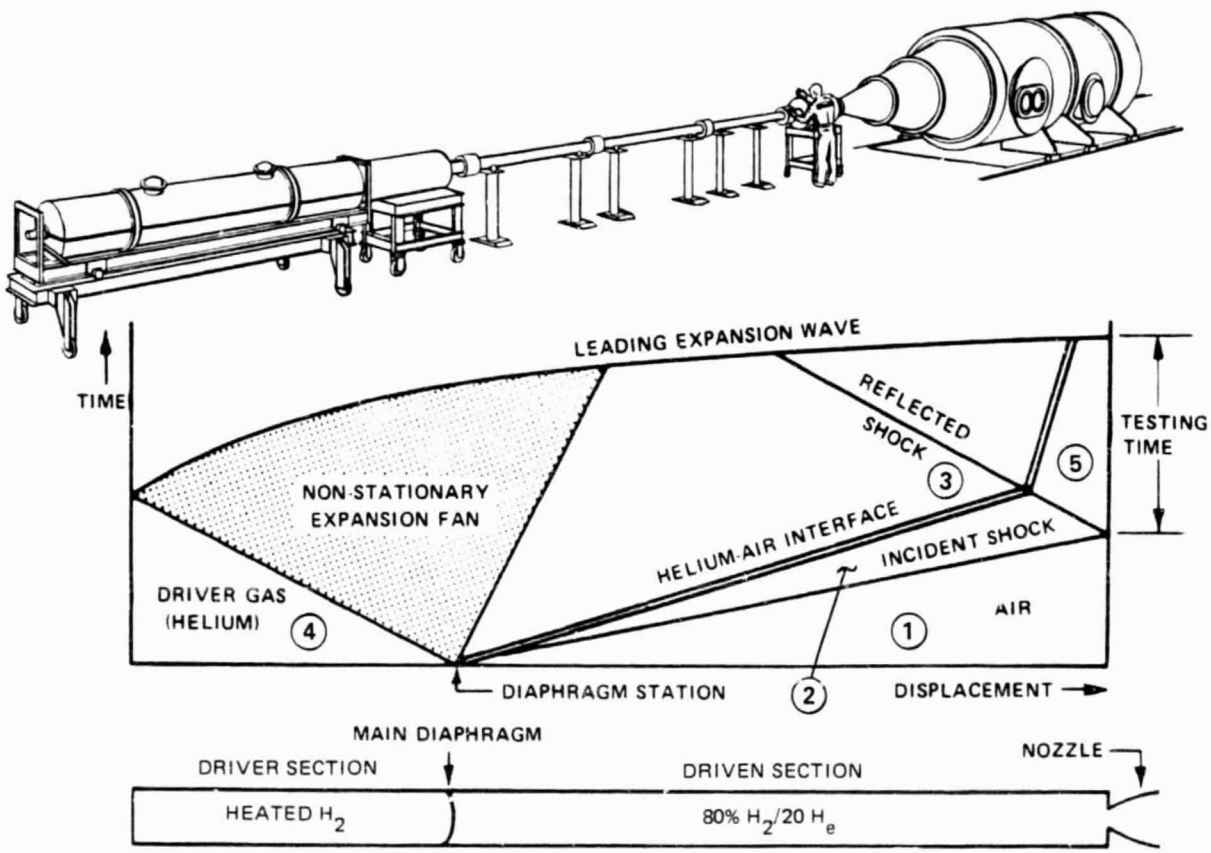

Figure 11 WAVE DIAGRAM FOR TAILORED-INTERFACE SHOCK TUBE

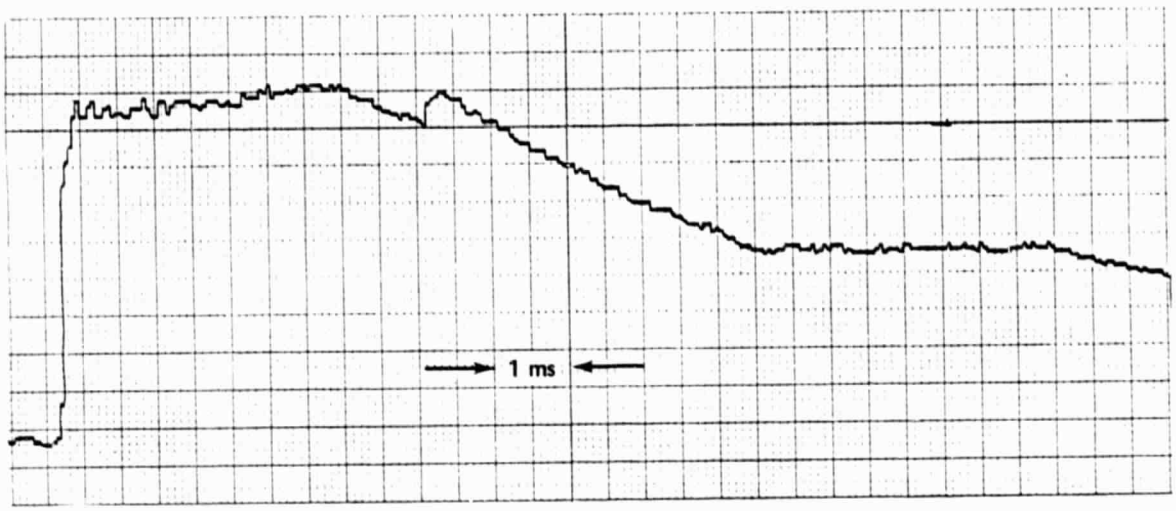

(a) RESERVOIR PRESSURE TRACE

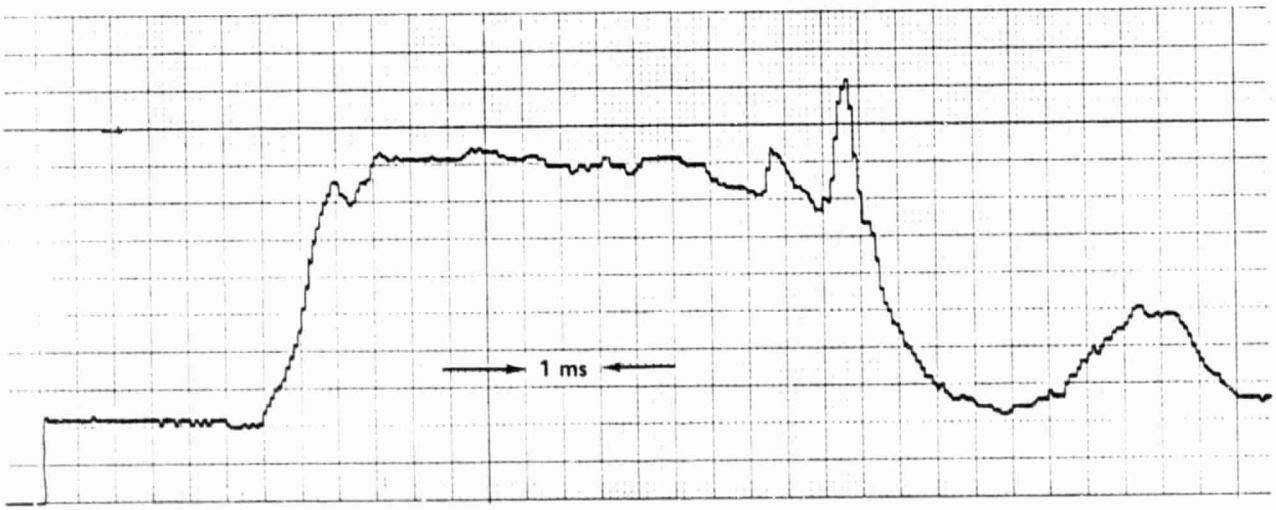

(b) PITOT PRESSURE TRACE

Figure 12 PRESSURE TIME HISTORIES

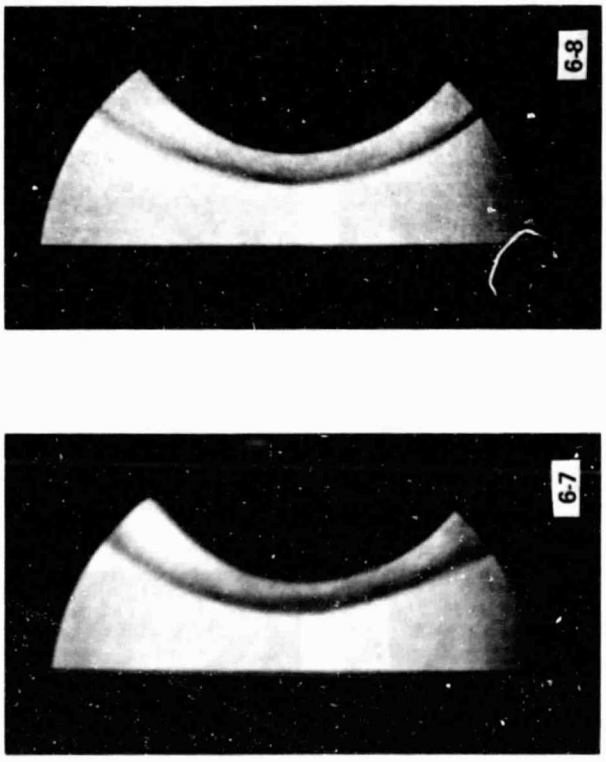

Figure 13 SCHLIEREN PHOTOGRAPHS WITH NO MASS FLOW

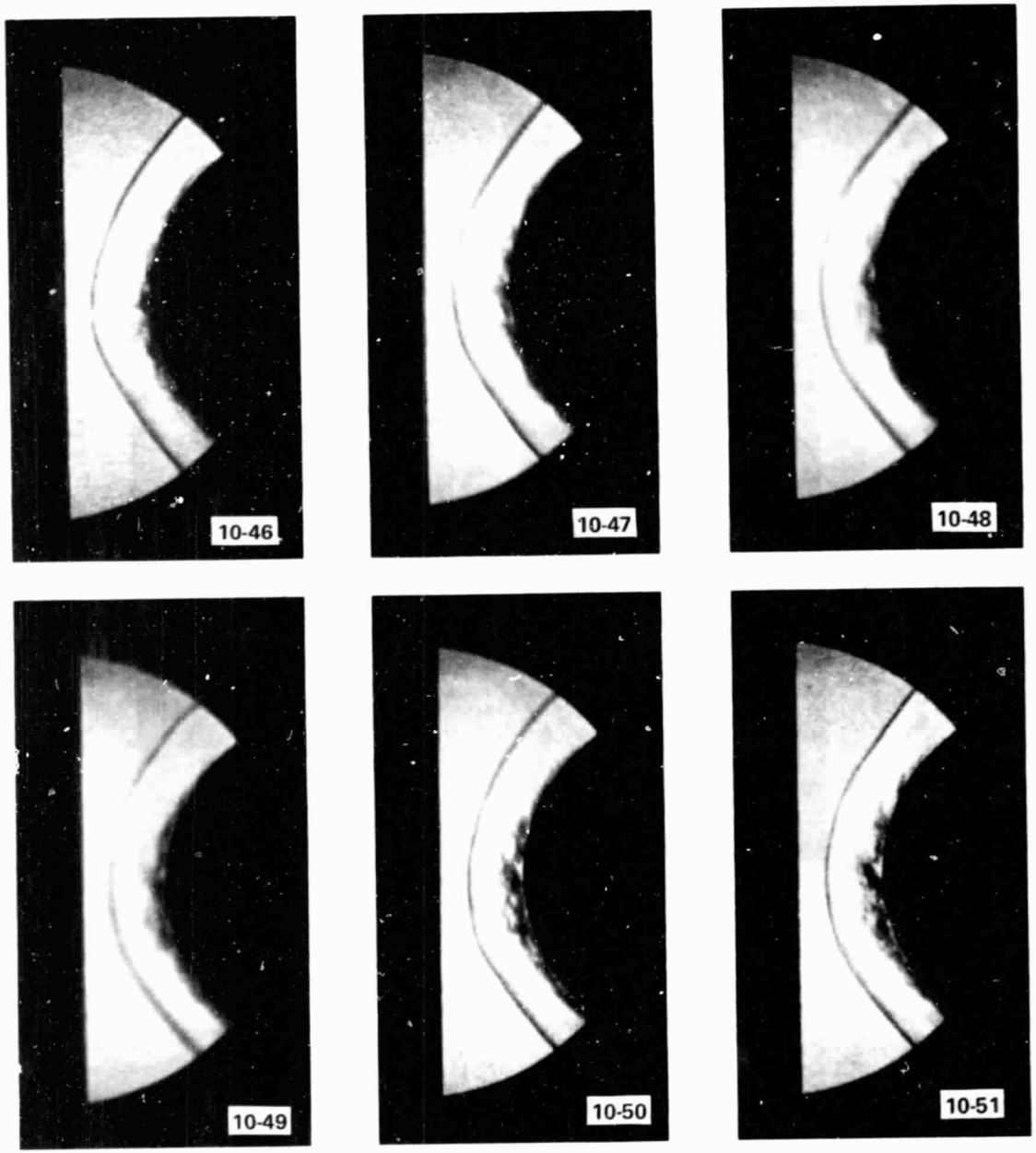

Figure 14 SCHLIEREN PHOTOGRAPHS OF FLOW WITH CF_4 INJECTION $\dot{m}/\rho_\infty u_\infty = 0.3$

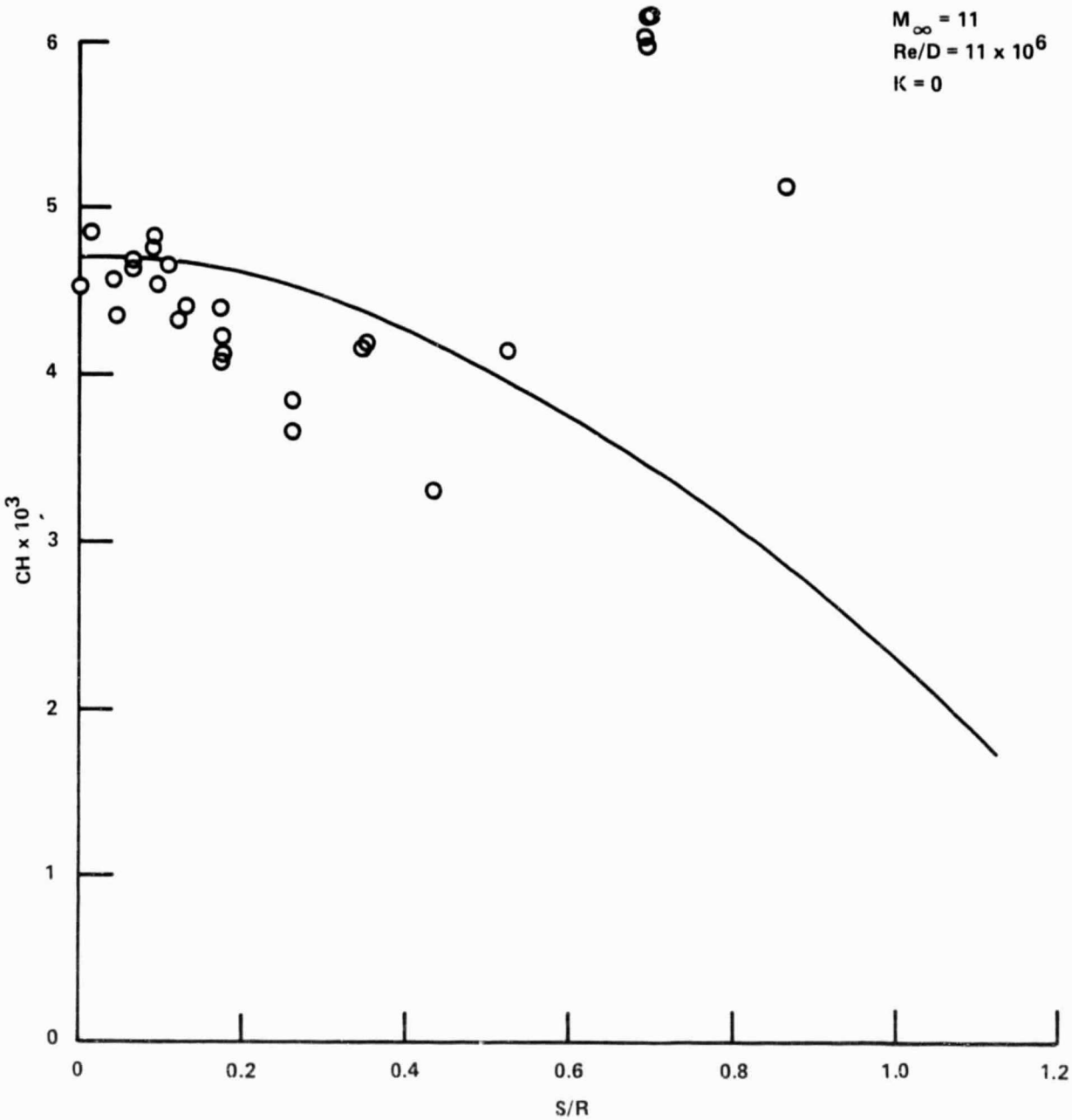

Figure 15 DISTRIBUTION OF HEAT TRANSFER TO SMOOTH HEMISPHERICAL NOSETIP

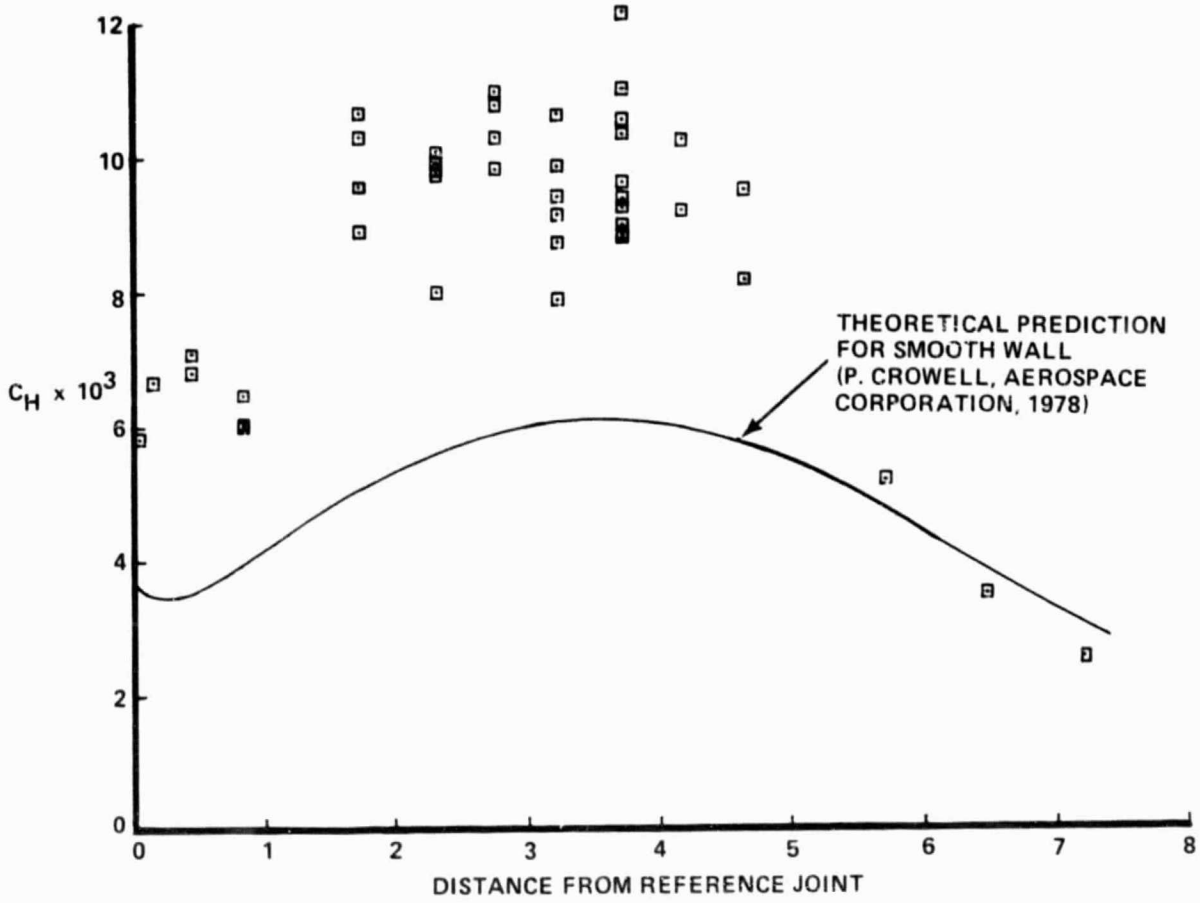

Figure 16 STREAMWISE DISTRIBUTION OF HEAT TRANSFER COEFFICIENT TO THE NOSE TIP FOR $\rho_w v_w / \rho_\infty U_\infty = 0$ ($M_\infty = 11.3$, $Re_D = 11.1 \times 10^7$)

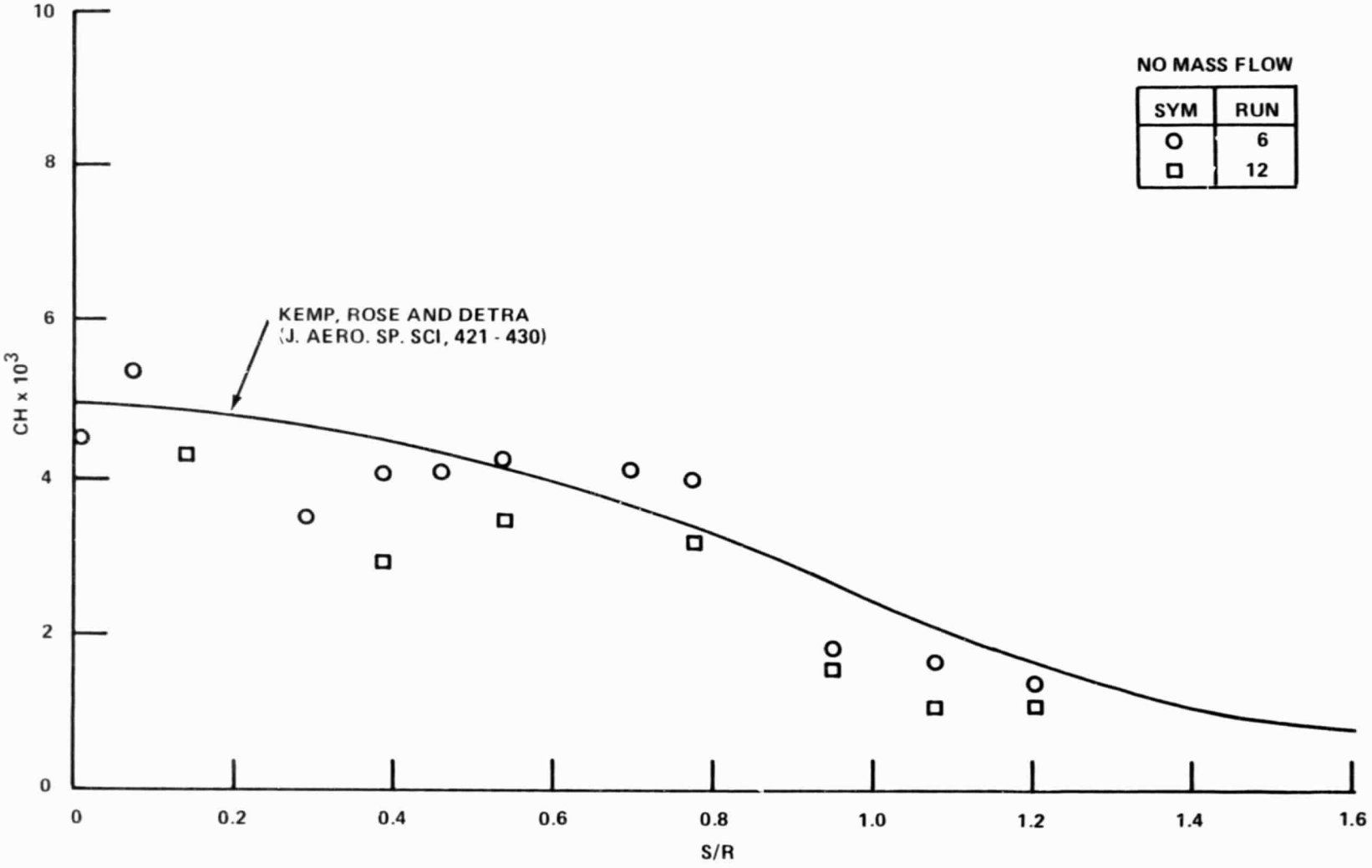

Figure 17 VARIATION OF DISTRIBUTION OF HEAT TRANSFER ON TCNT WITH NO MASS FLOW

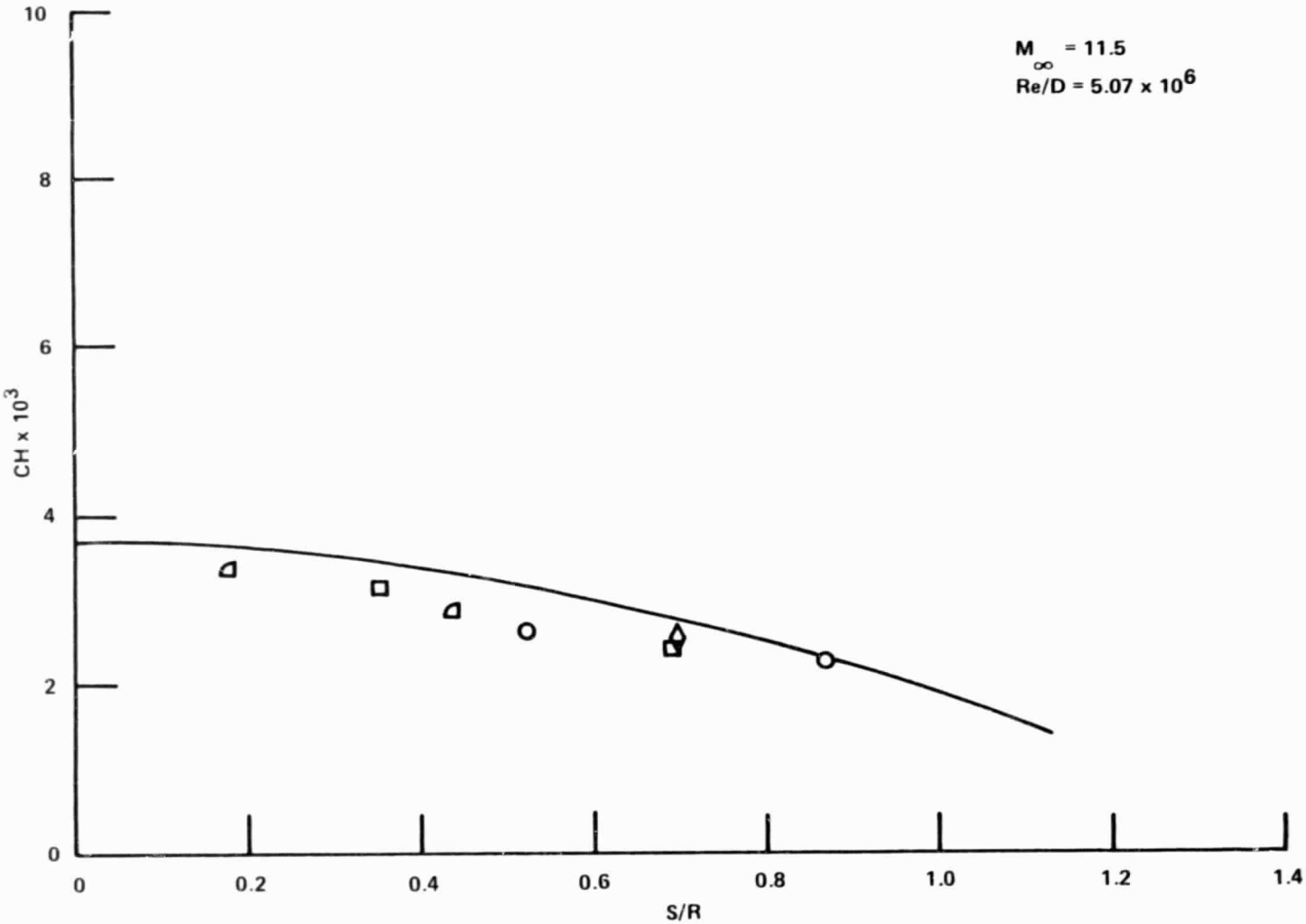

Figure 18 HEAT TRANSFER DISTRIBUTION TO THE SMOOTH REPLICA OF THE TRANSPIRATION COOLED NOSETIP

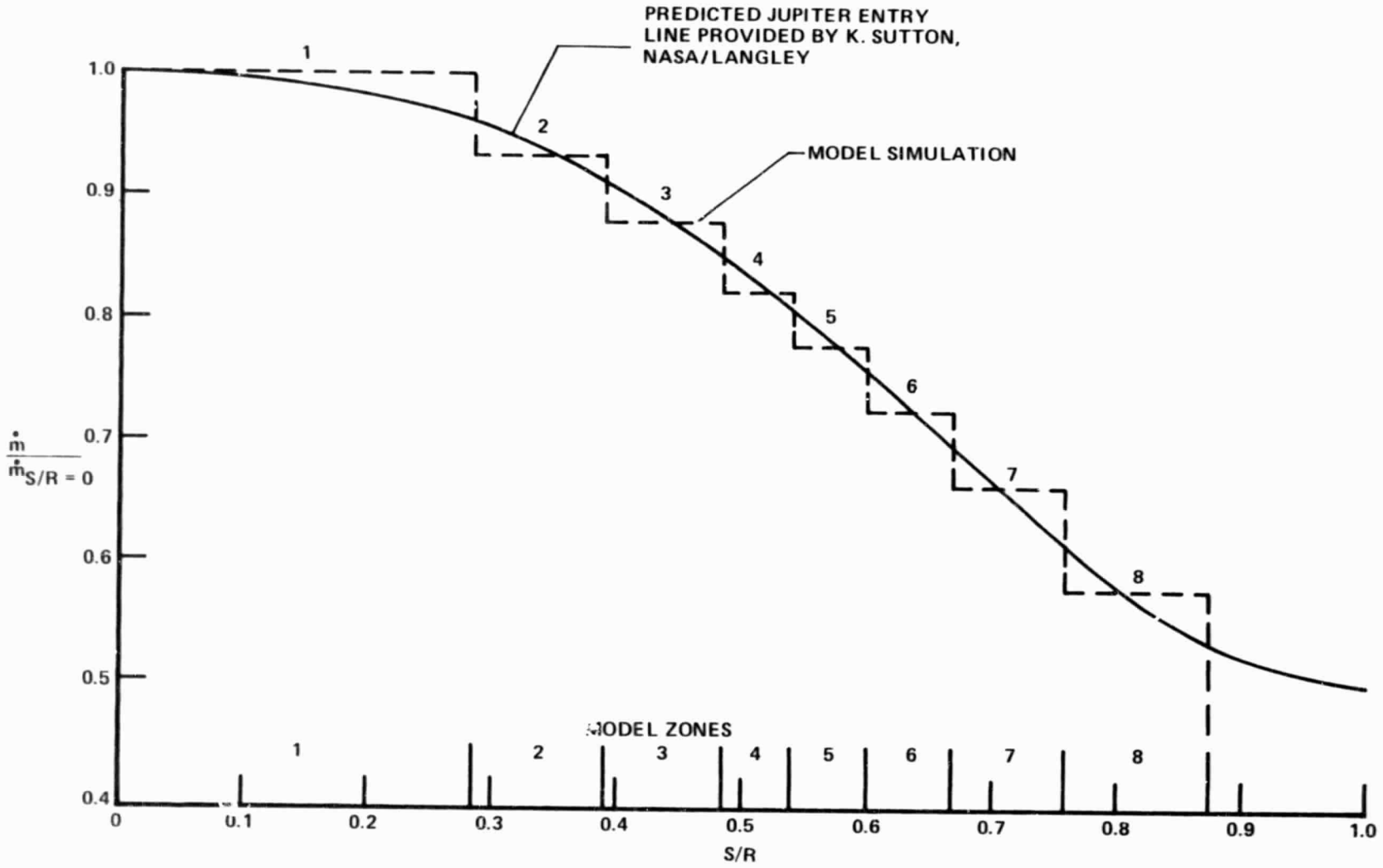

Figure 19 MASS INJECTION DISTRIBUTION

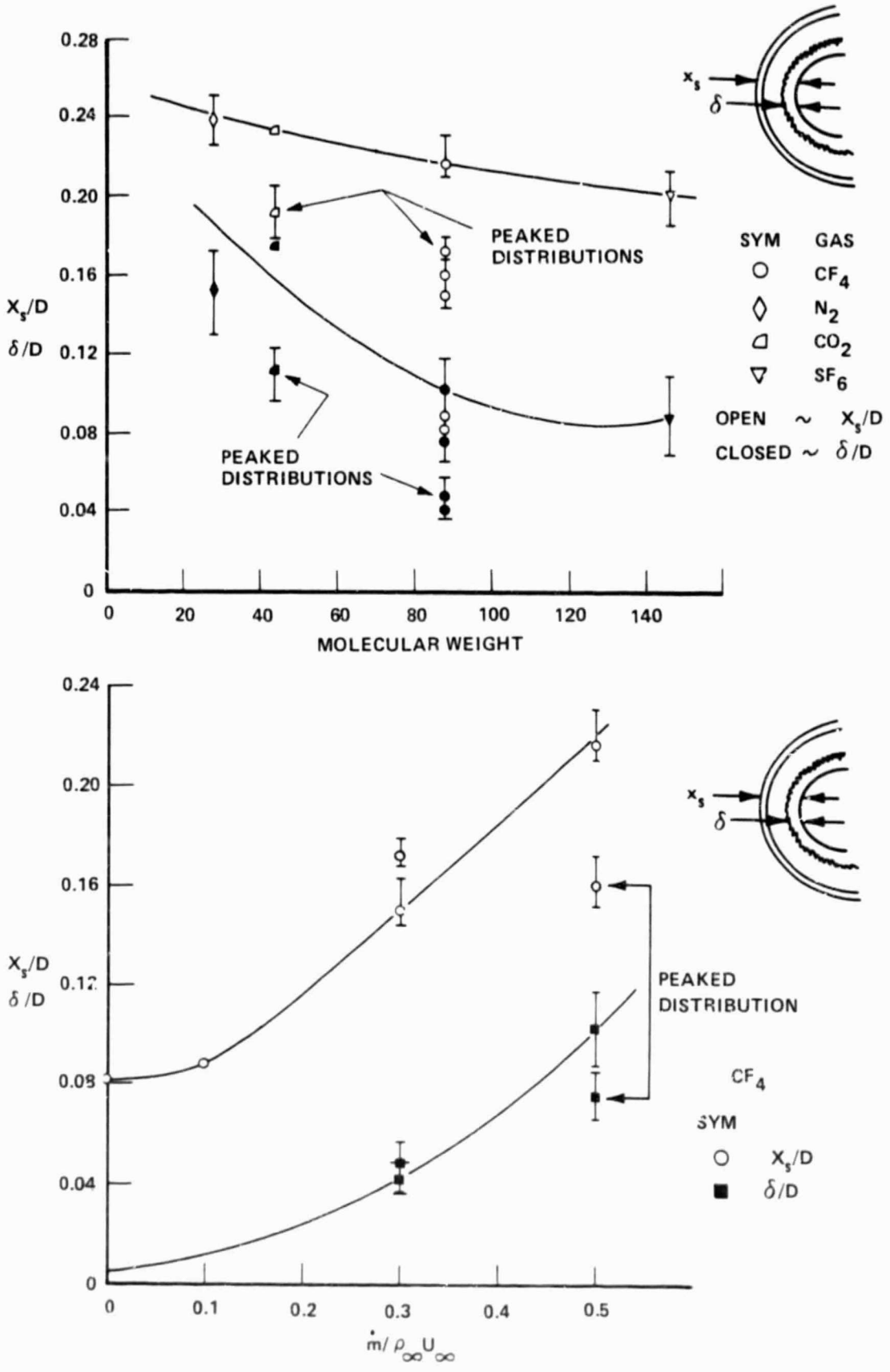

Figure 20 VARIATION OF SHOCK STANDOFF DISTANCE & MIXING LAYER THICKNESS WITH MASS INJECTION RATE AND MOLECULAR WEIGHT OF INJECTION

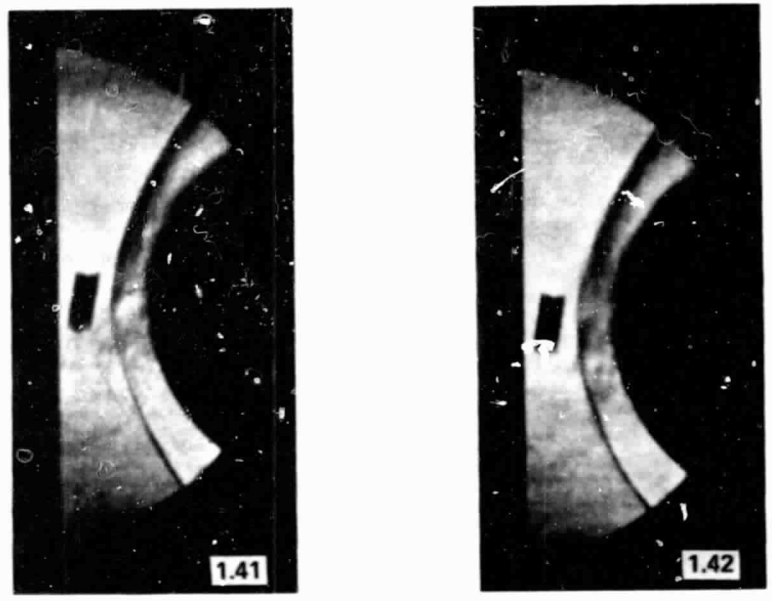

Figure 21 SCHLIEREN PHOTOGRAPHS OF FLOW WITH CF_4 INJECTION $\dot{m}/\rho_\infty u_\infty = 0.1$

Figure 22 SCHLIEREN PHOTOGRAPHS OF FLOW WITH CF_4 INJECTION $\dot{m}/\rho_\infty u_\infty = 0.3$

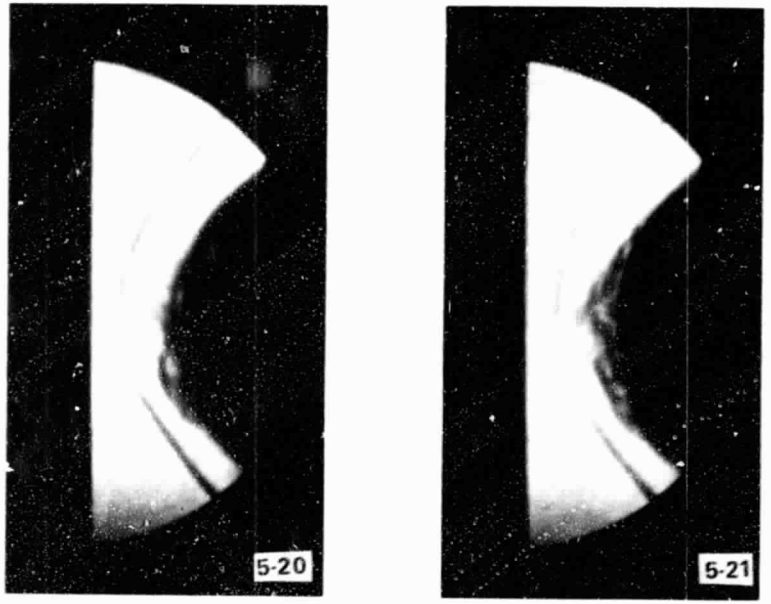

Figure 23 SCHLIEREN PHOTOGRAPHS OF FLOW WITH CO_2 (PEAKED) INJECTION $\dot{m}/\rho_\infty u_\infty = 0.5$

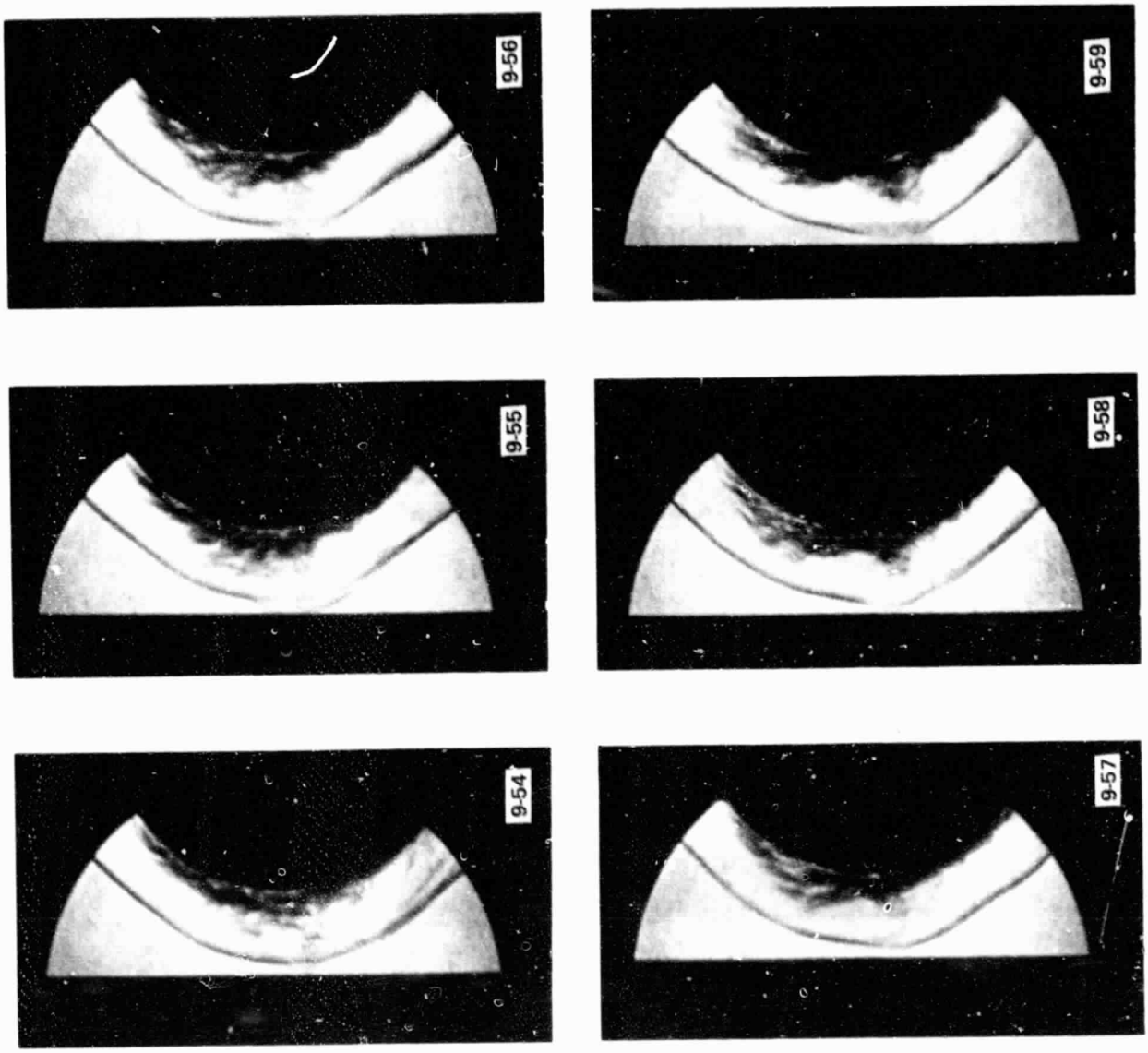

Figure 24 SCHLIEREN PHOTOGRAPHS OF FLOW WITH CF_4 INJECTION $\dot{m}/\rho_\infty u_\infty = 0.5$

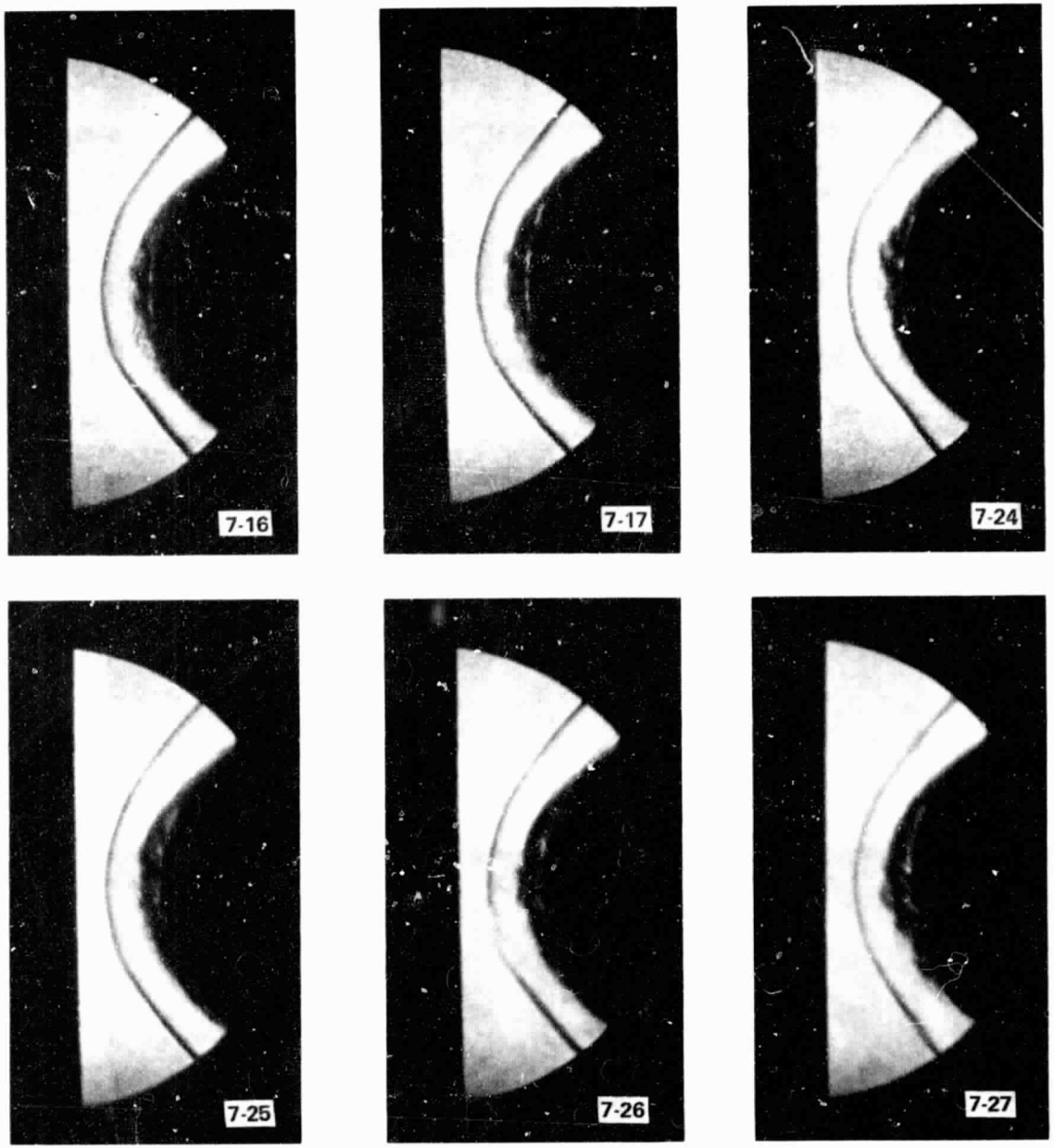

Figure 25 SCHLIEREN PHOTOGRAPHS OF FLOW WITH CF_4 (PEAKED) INJECTION
$\dot{m}/\rho_\infty u_\infty = 0.5$

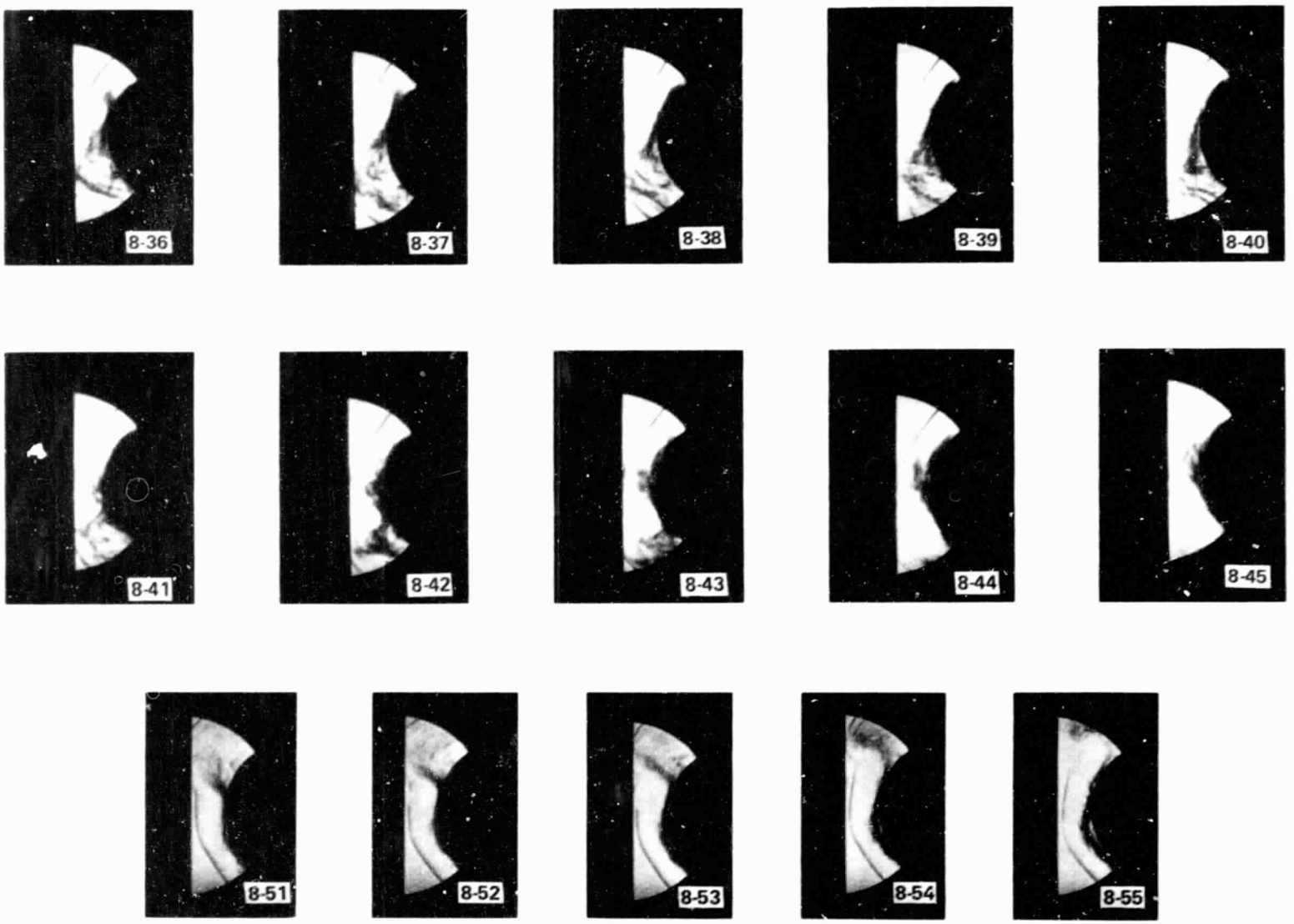

Figure 26 SCHLIEREN PHOTOGRAPHS OF FLOW WITH CF_4 (PEAKED) INJECTION
$\dot{m}/\rho_\infty u_\infty = 0.7$

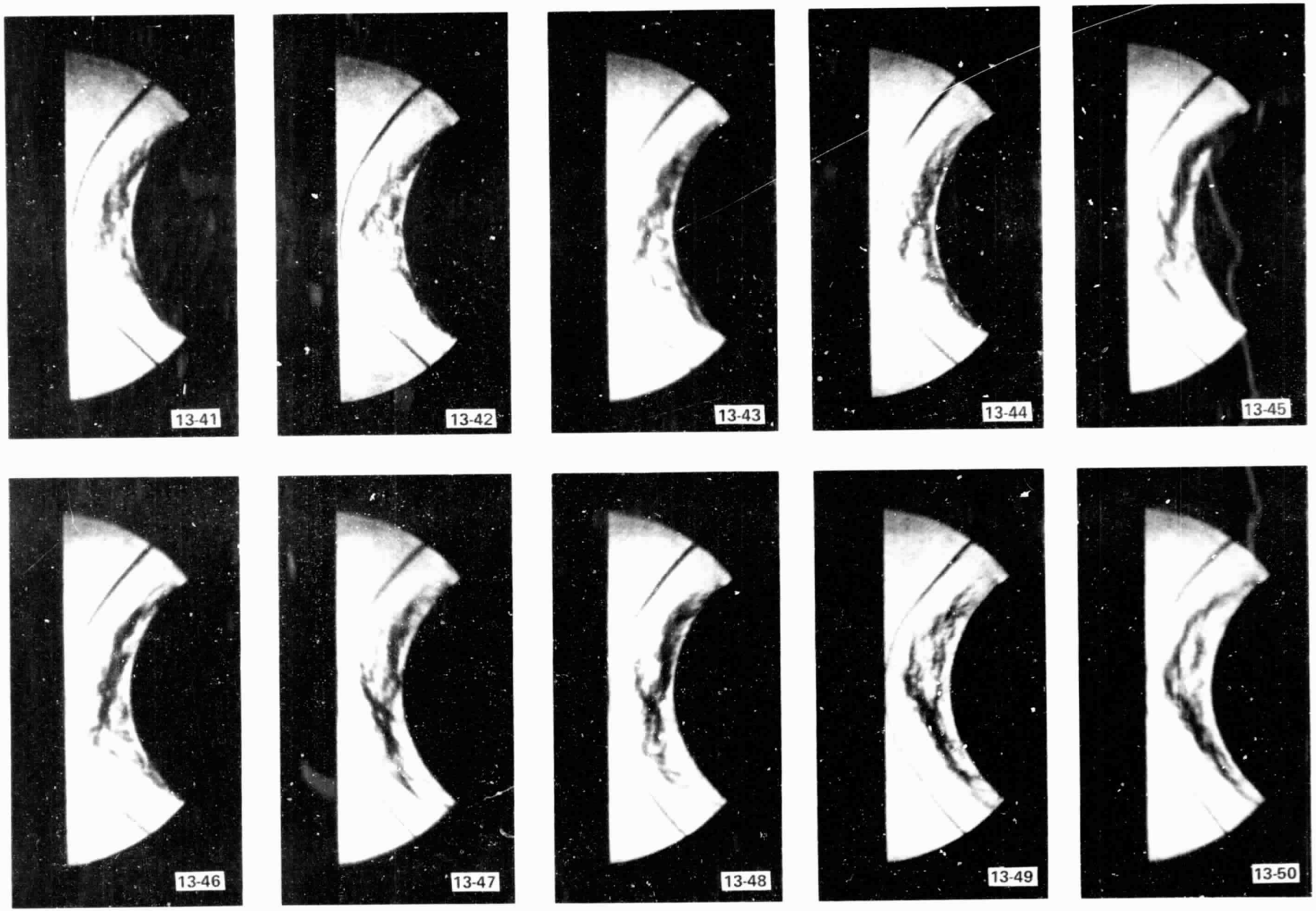

Figure 27 SCHLIEREN PHOTOGRAPHS OF FLOW WITH N_2 INJECTION $\dot{m}/\rho_\infty u_\infty = 0.5$

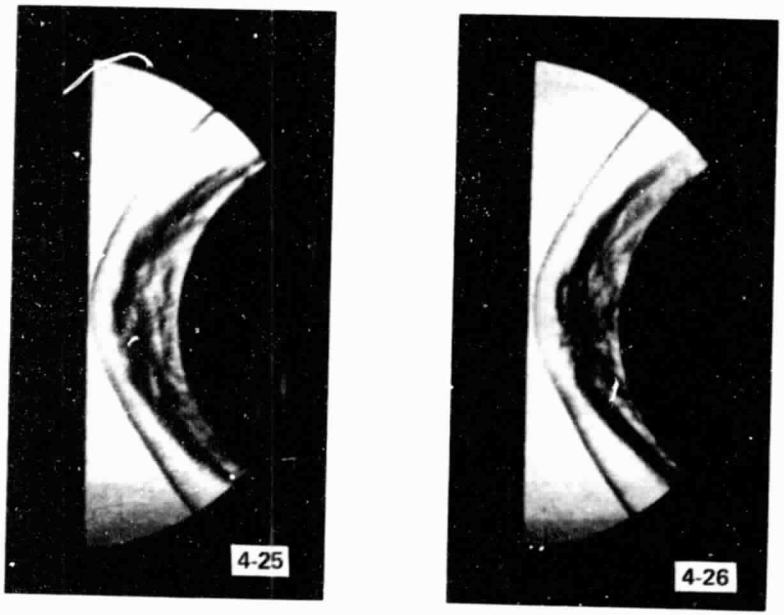

Figure 28 SCHLIEREN PHOTOGRAPHS OF FLOW WITH CO_2 (UNIFORM) INJECTION
$\dot{m}/\rho_\infty u_\infty = 0.5$

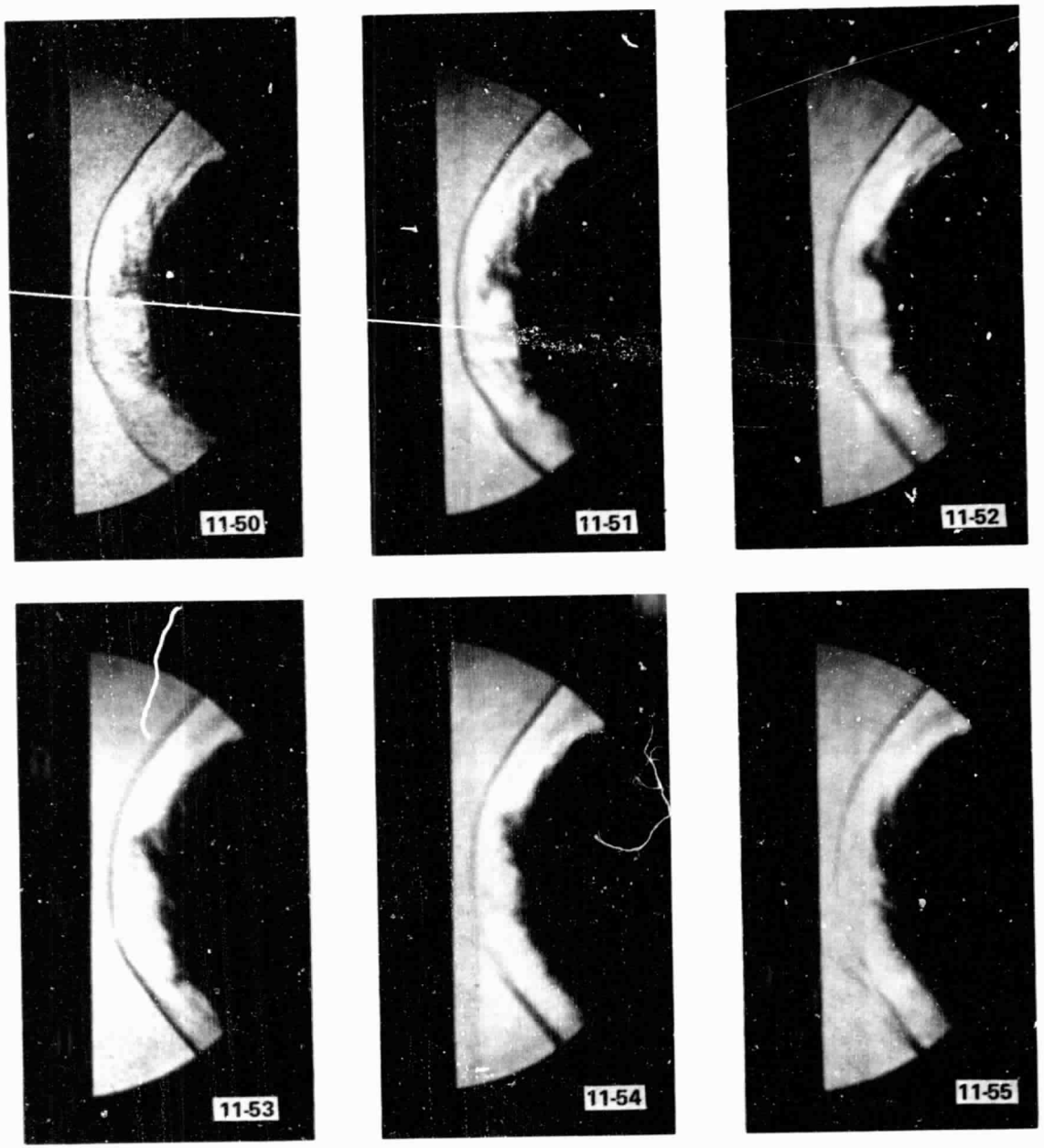

Figure 29 SCHLIEREN PHOTOGRAPHS OF FLOW WITH SF_6 INJECTION $\dot{m}/\rho_\infty u_\infty = 0.5$

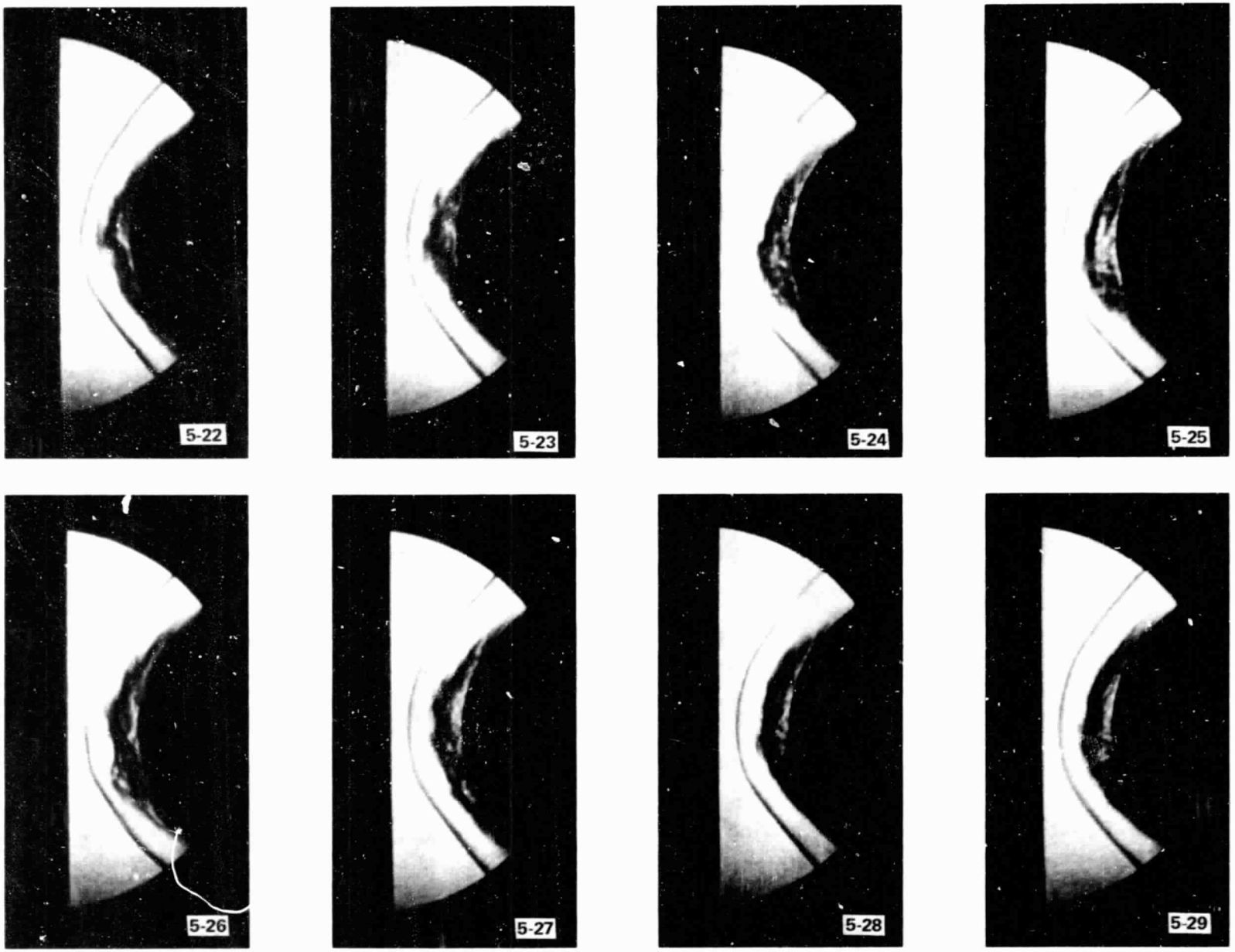

Figure 30a SCHLIEREN PHOTOGRAPHS OF FLOW WITH CO_2 (PEAKED) INJECTION

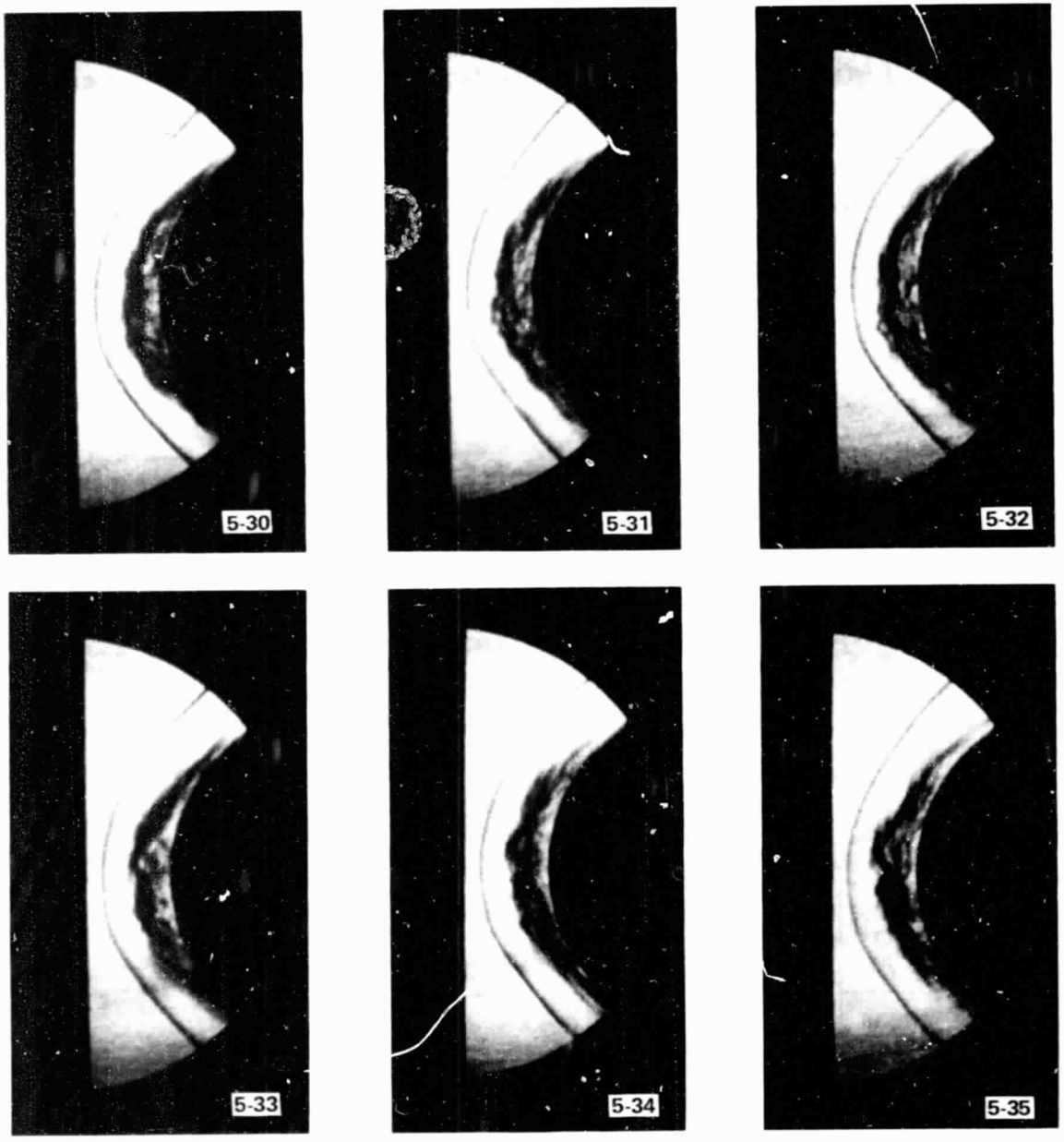

Figure 30b SCHLIEREN PHOTOGRAPHS OF FLOW WITH CO_2 (PEAKED) INJECTION $\dot{m}/\rho_\infty u_\infty = 0.5$ (CONT.)

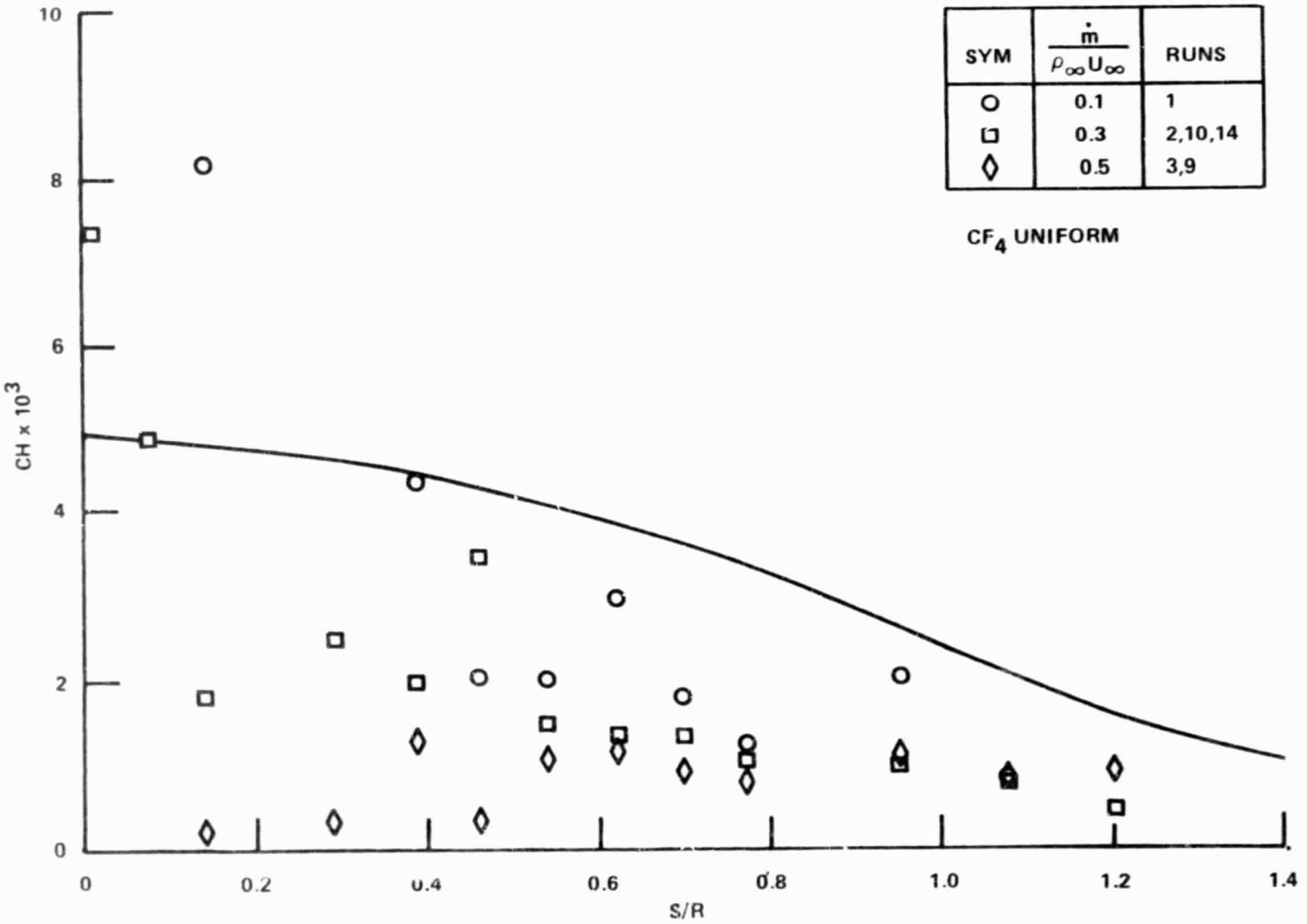

Figure 31 VARIATION OF DISTRIBUTION OF HEAT TRANSFER ON TCNT WITH BLOWING RATE FOR UNIFORM CF_4 INJECTION

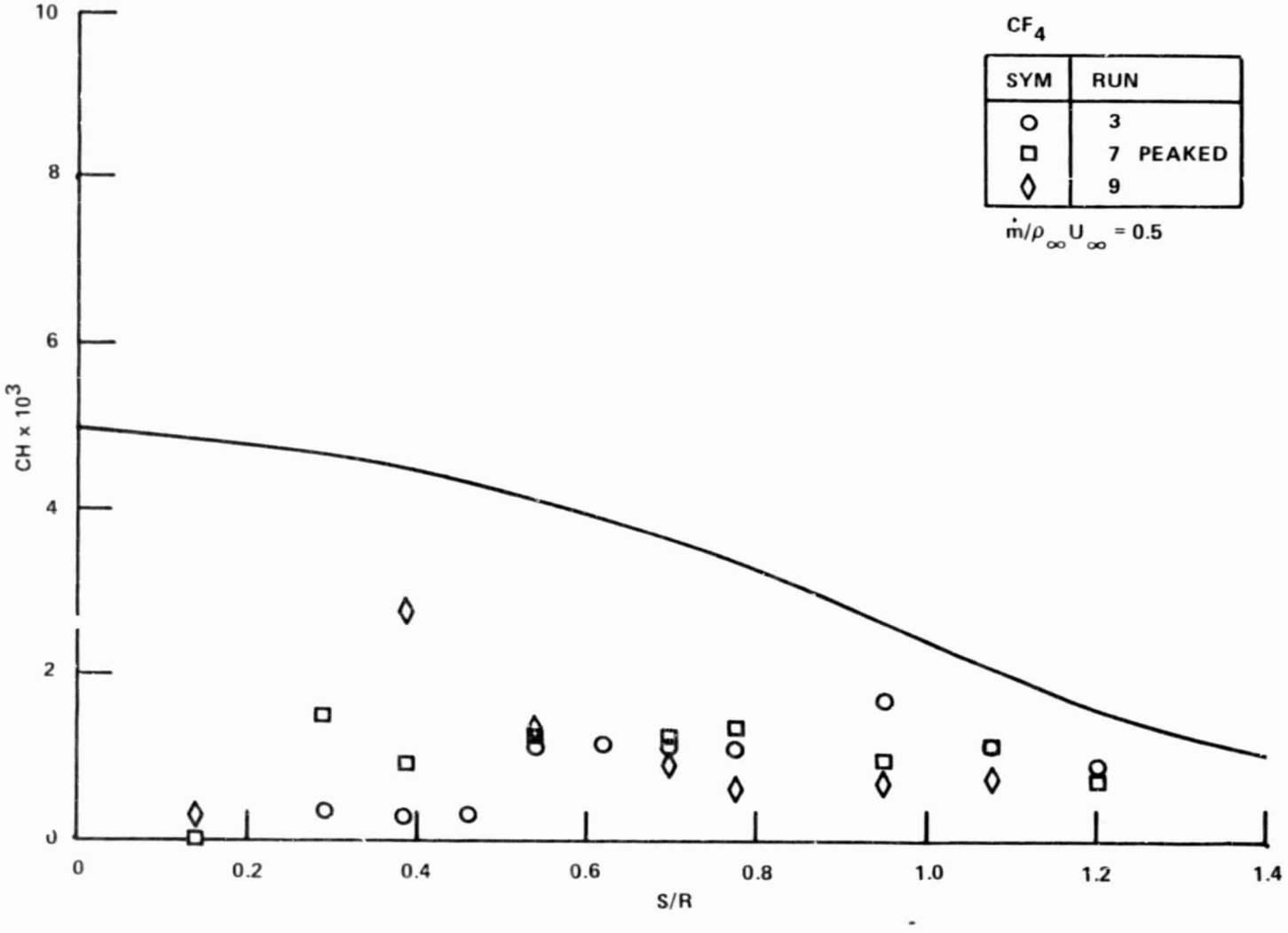

Figure 32 DISTRIBUTION OF HEATING OVER TCNT WITH UNIFORM AND PEAKED INJECTION WITH CF_4 FOR $(\dot{m}/\rho_\infty U_\infty)_{MAX} = 0.5$

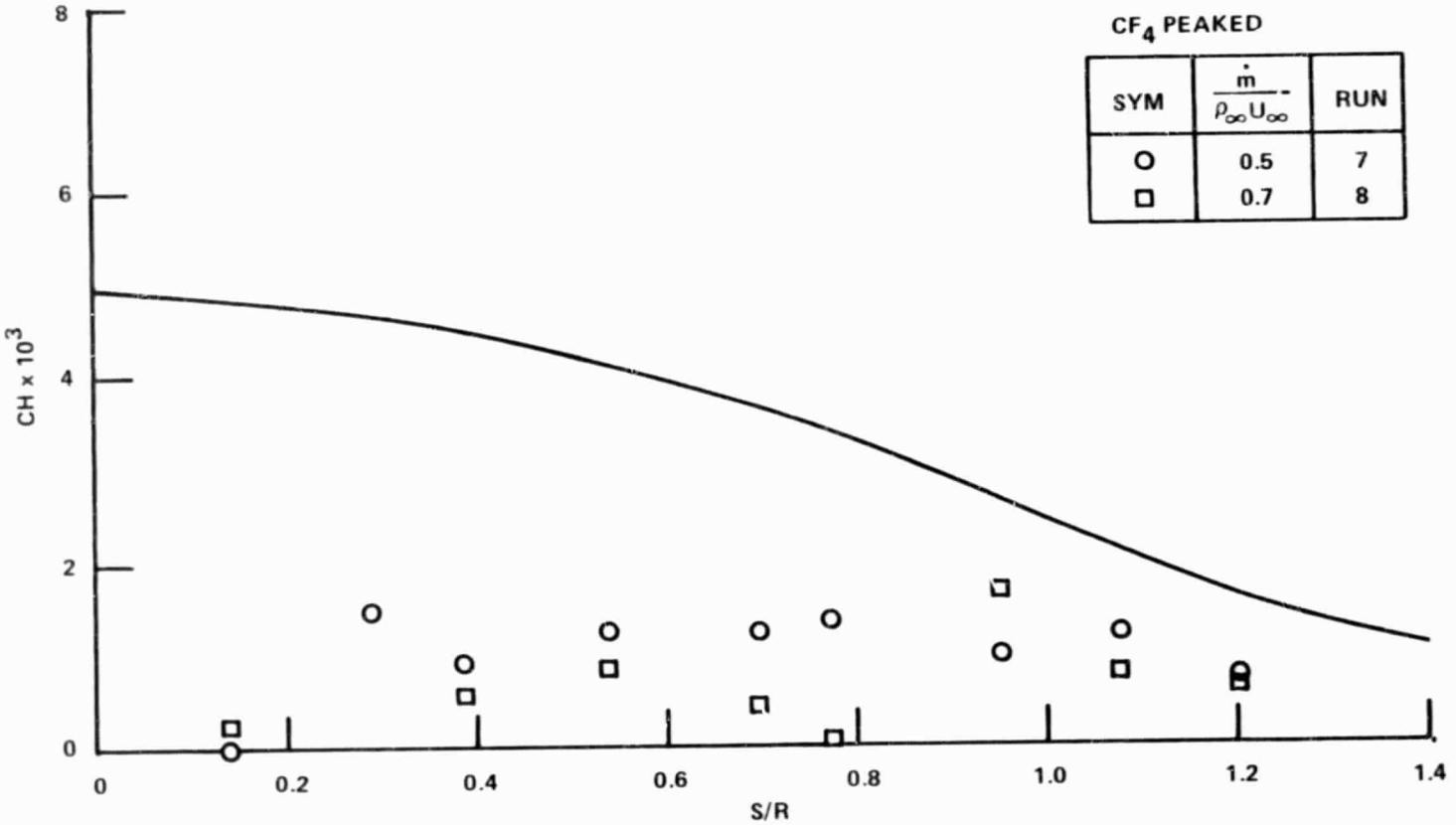

Figure 33 DISTRIBUTION OF AVERAGE HEAT TRANSFER FOR PEAKED CF_4 INJECTION RATES OF $\dot{m}/\rho_\infty U_\infty$ = 0.5 AND 0.7

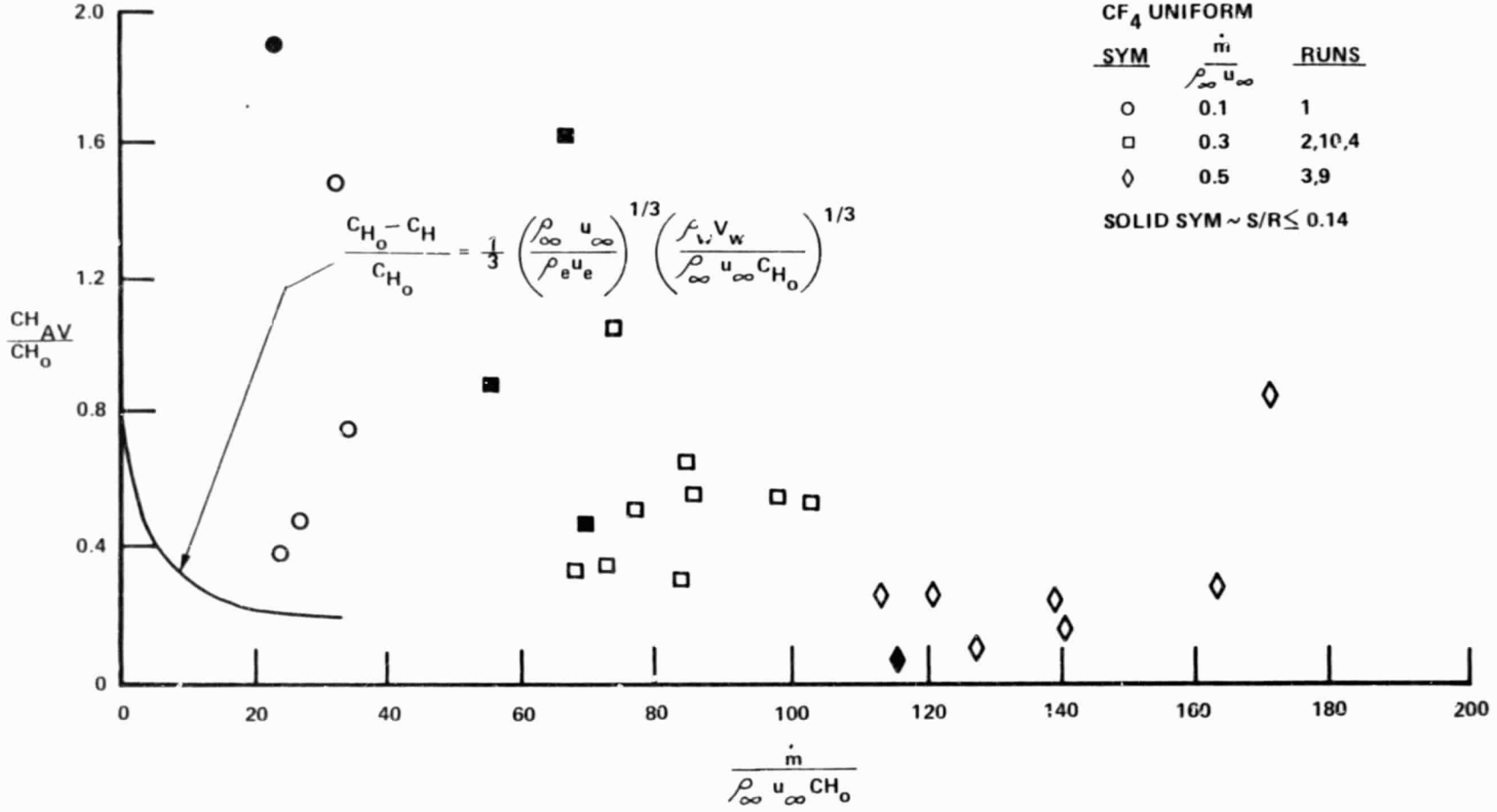

Figure 34 VARIATION OF NON-DIMENSIONAL HEATING RATE WITH BLOWING PARAMETER FOR UNIFORM CF_4 INJECTION

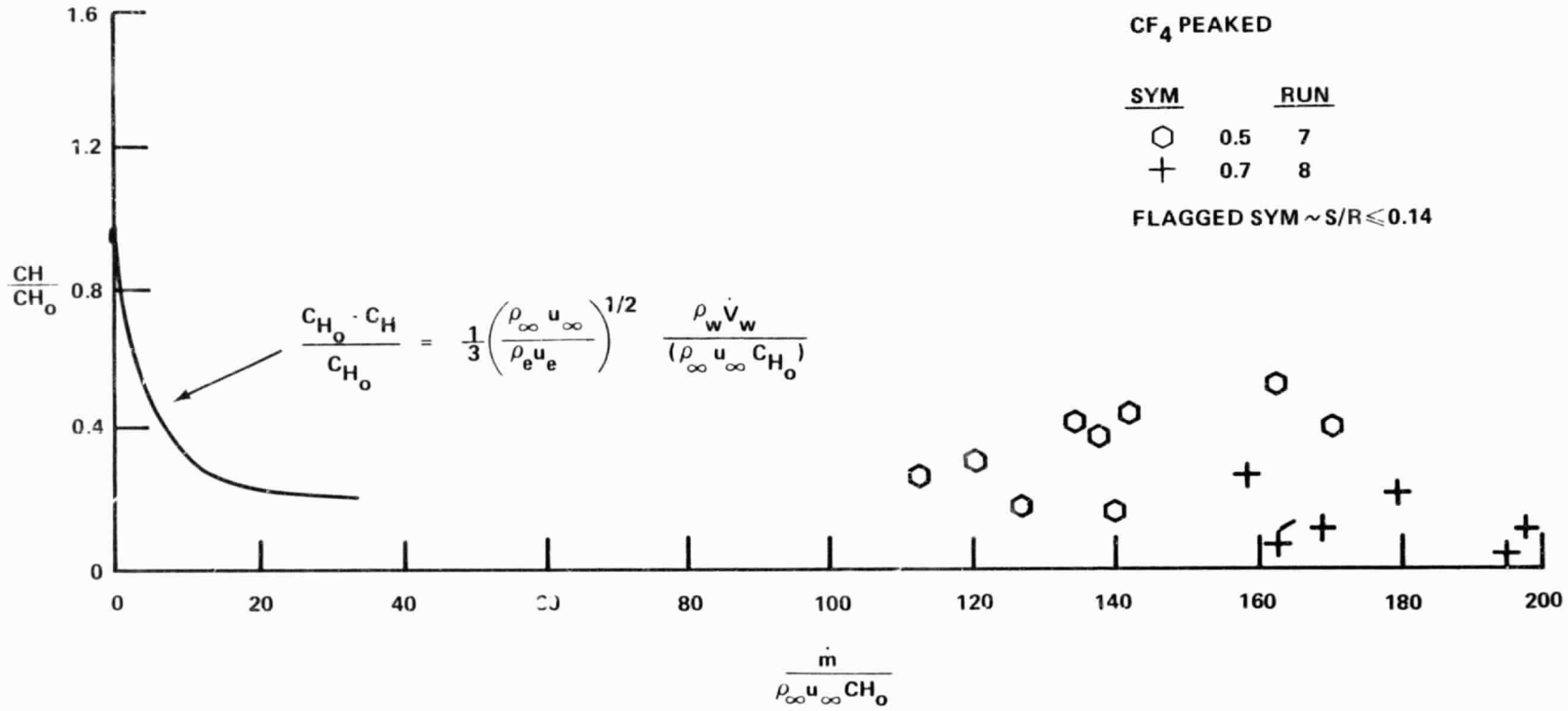

Figure 35 VARIATION OF NON-DIMENSION HEATING WITH BLOWING PARAMETER FOR CF_4 PEAKED INJECTION

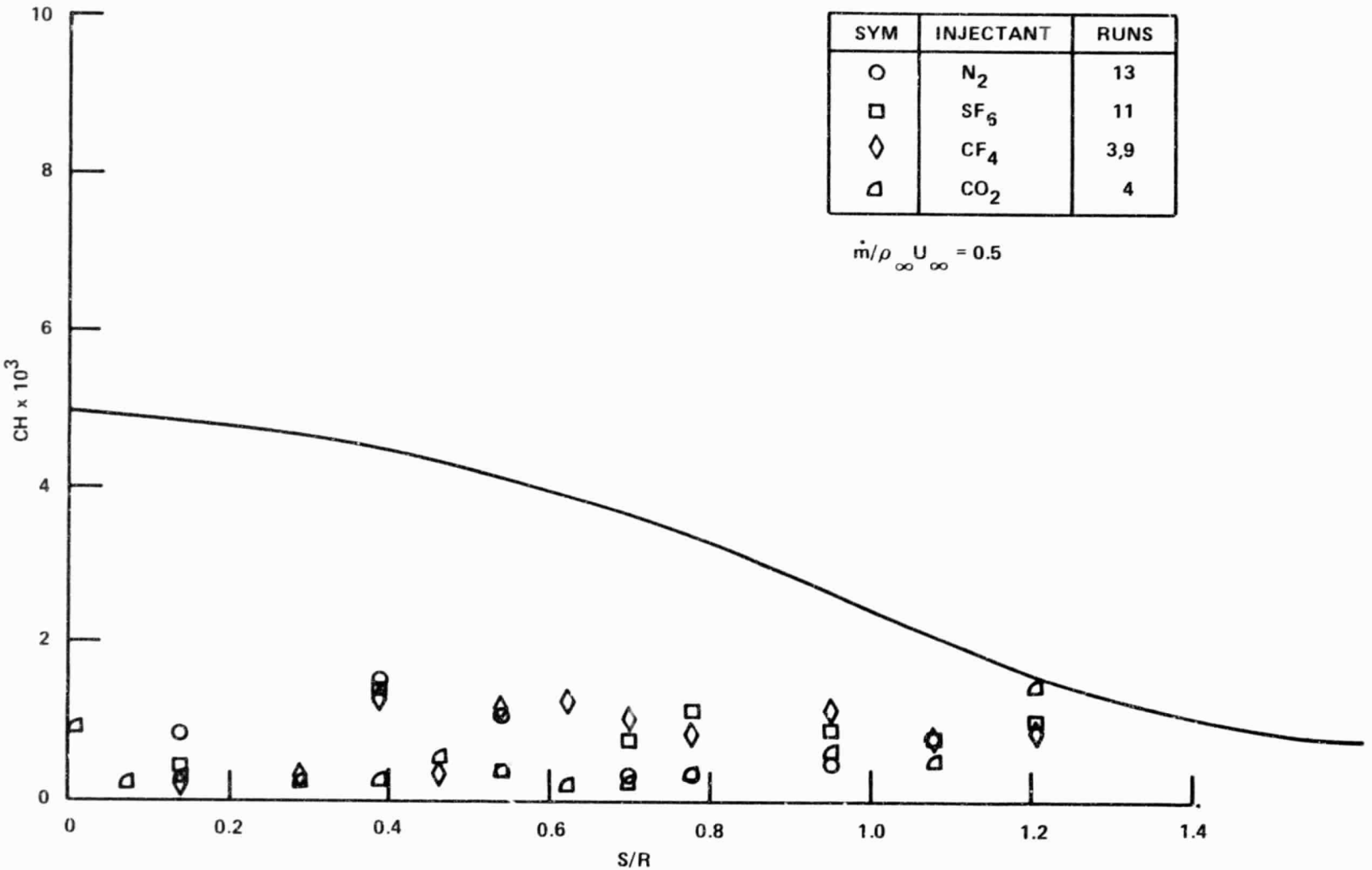

Figure 36 VARIATION OF HEAT TRANSFER DISTRIBUTION ON TCNT WITH MOLECULAR WEIGHT OF INJECTANT FOR $\dot{m}/\rho_\infty U_\infty = 0.5$

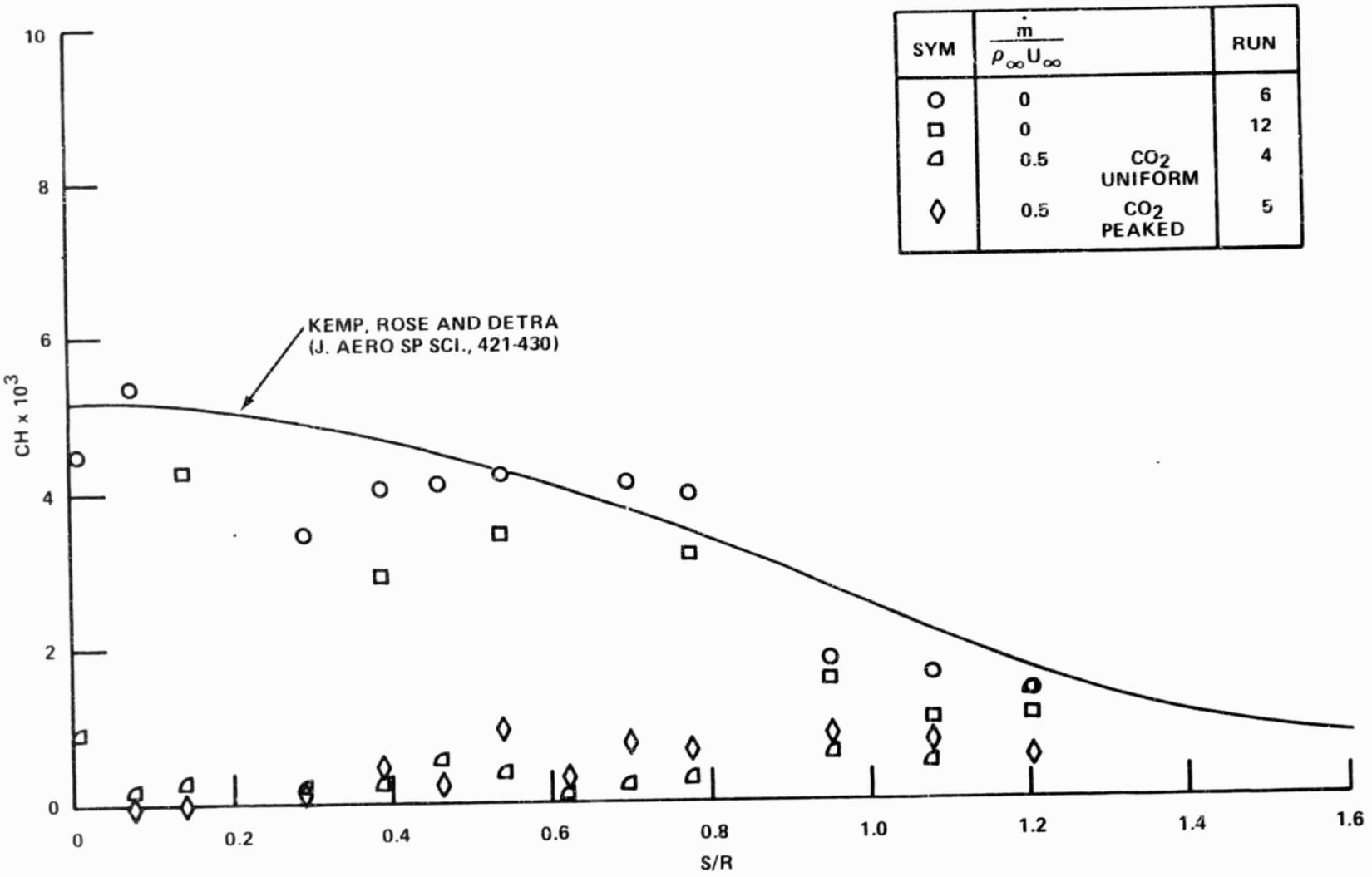

Figure 37 VARIATION OF HEAT TRANSFER DISTRIBUTION ON TCNT WITH MOLECULAR WEIGHT INJECTION FOR $\dot{m}/\rho_\infty U_\infty = 0.5$

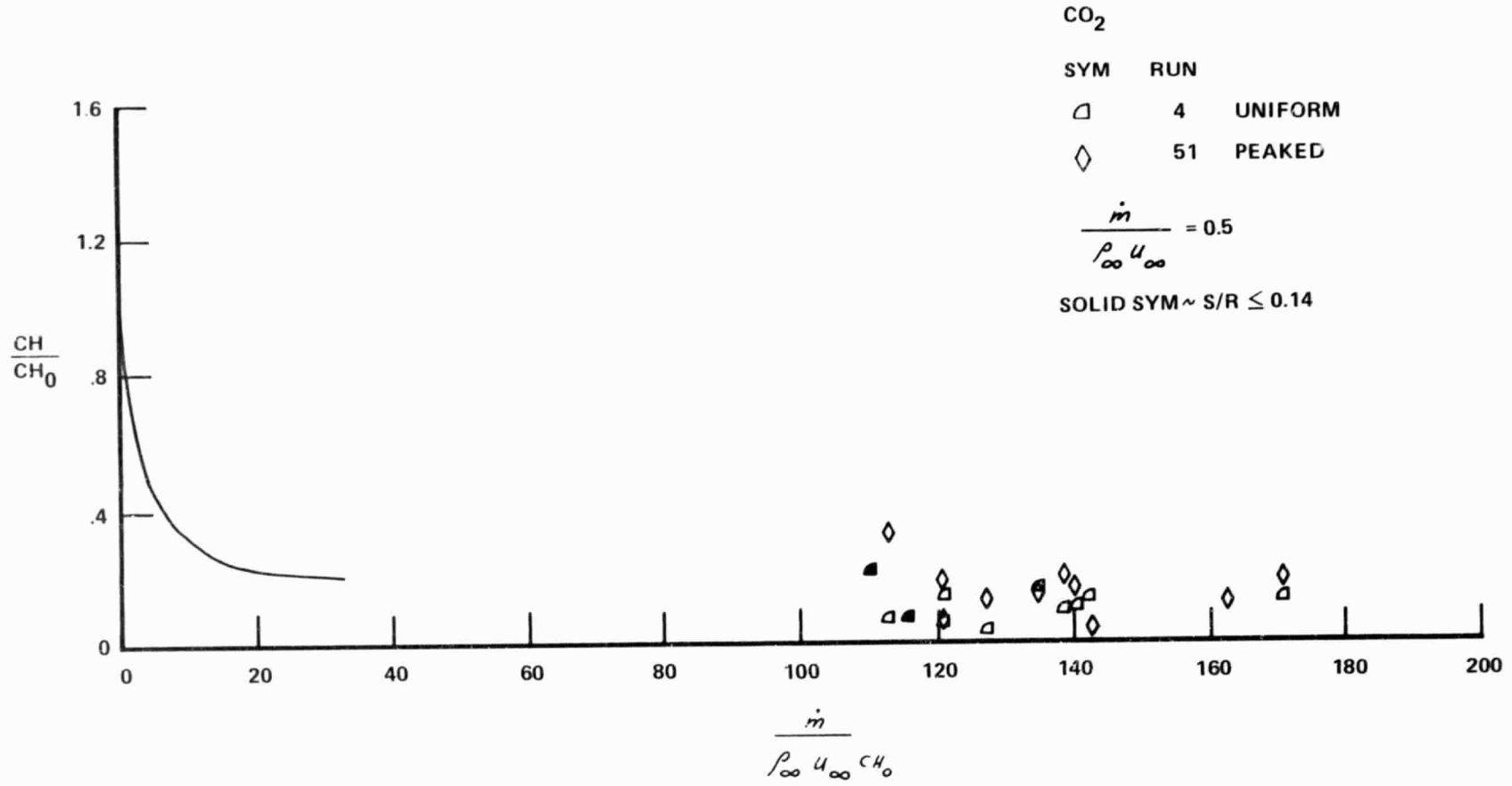

Figure 38 VARIATION OF NONDIMENSIONAL HEATING WITH BLOWING PARAMETER FOR UNIFORM AND PEAKED CO_2 INJECTION